Matthias Ehrhart

Automated, Total Station-based Verification of Reflector Pole Heights

MASTERARBEIT

zur Erlangung des akademischen Grades
Diplom-Ingenieur/in

Masterstudium Geomatics Science

Technische Universität Graz

Betreuer:

Univ.-Prof. Dipl.-Ing. Dr.techn. Werner Lienhart

Institut für Ingenieurgeodäsie und Messsysteme

Graz, September 2012

Deutsche Fassung:
Beschluss der Curricula-Kommission für Bachelor-, Master- und Diplomstudien vom 10.11.2008
Genehmigung des Senates am 1.12.2008

EIDESSTATTLICHE ERKLÄRUNG

Ich erkläre an Eides statt, dass ich die vorliegende Arbeit selbstständig verfasst, andere als die angegebenen Quellen/Hilfsmittel nicht benutzt, und die den benutzten Quellen wörtlich und inhaltlich entnommene Stellen als solche kenntlich gemacht habe.

Graz, am ……. ……..
(Unterschrift)

Englische Fassung:

STATUTORY DECLARATION

I declare that I have authored this thesis independently, that I have not used other than the declared sources / resources, and that I have explicitly marked all material which has been quoted either literally or by content from the used sources.

……. ……..
date (signature)

Abstract

In this thesis, the prototype of a system for the automatic detection of wrong reflector pole heights has been developed. The system is based on measurements of the total station (Leica TS15) so that no additional sensors are required at the reflector pole. The heights are determined by using the total station's automatic target recognition (ATR) and its wide-angle camera (WAC). With the proposed method, it is possible to automatically determine the reflector pole height with an accuracy of better than 5 mm for distances up to 550 m. Finally, possible improvements of the prototype are discussed with suggestions for a cost-efficient production of a market-ready system.

Kurzfassung

In dieser Masterarbeit wird der Prototyp eines Systems für die automatische Erkennung von falsch eingegebenen Reflektorhöhen bei Messungen mit Lotstöcken vorgestellt. Für die Messungen werden ausschließlich die Sensoren einer Totalstation (Leica TS15) verwendet, d.h. es sind keine zusätzlichen Sensoren am Lotstock notwendig. Für die Messung der Höhen werden die automatische Zielerkennung (automatic target recognition, ATR) sowie die Weitwinkelkamera (wide-angle camera, WAC) der Totalstation verwendet. Das vorgestellte System wurde für Distanzen bis zu 550 m getestet wobei die gemessenen Höhen Fehler von weniger als 5 mm aufwiesen. Abschließend werden mögliche Weiterentwicklungen des Prototypen diskutiert, wobei auch Vorschläge für die kostengünstige Entwicklung eines marktreifen Produktes gemacht werden.

Acknowledgements

Univ.-Prof. Dipl.-Ing. Dr.techn. Werner Lienhart (Institute of Engineering Geodesy and Measurement Systems, TU Graz) I want to thank for the motivating support throughout the work on this thesis. His detailed explanations on the operating principle of modern total stations enabled me to interpret some of the discovered effects.

Ing. Rudolf Lummerstorfer and Dipl.-Ing. (FH) Robert Presl (Institute of Engineering Geodesy and Measurement Systems, TU Graz) I want to thank for assisting me in the experiments made in the Geodetic Metrology Laboratory.

Dipl.-Ing. Dr.techn. Karlheinz Gutjahr (Institute of Digital Image Processing, Joanneum Research Graz) and Christian Sommer deserve thanks for explanations on the operating principle of digital cameras.

Dipl.-Ing. Andreas Wendel (Institute for Computer Graphics and Vision, TU Graz) I want to thank for giving me valuable advices for the implementation and improvement of the marker detection routine.

Dagmar Tschabrun assisted me in many practical measurements. Furthermore, she showed a huge understanding for me being working late at night - especially during the completion of this thesis but also in the past four years.

Finally, I want to thank my parents Maria and Martin. They offered me a childhood free of sorrows and supported my education from kindergarten to university.

Contents

1 Introduction

1.1 Motivation

In tachymetric surveying, total stations are used to determine the coordinates of objects by polar measurements (direction, zenith angle and slope distance) from a point with known coordinates. The polar elements refer to a prism mounted on top of a reflector pole but the object, whose coordinates are of interest, refers to ground level. The height of the object is computed by subtracting the reflector pole height from the z-component of the prism's coordinates. Accordingly, an error in the reflector pole height directly falsifies the object's height.

In most cases, a tachymetric surveying is done by two persons where one person carries the reflector pole and the other person operates the total station. These two persons are commonly referred to as "assistant" and "observer". If an object obstructs the sighting between the total station and the prism, the assistant changes the reflector pole height and notifies the observer of the new height (typically via a radio connection). Before executing the polar measurement, the observer manually sets the new reflector pole height in the total station's user interface. This height is applied to the z-coordinates of all subsequently measured points.

There are numerous reasons for wrongly set reflector pole heights. Examples are loud noise (e.g. at construction sites or near streets) complicating the communication between the assistant and the observer, the assistant changing the reflector pole height without notifying the observer or transposed digits either in the read (by the assistant) or in the entered (by the observer) height. Except for mistakes in the communication between the assistant and the observer, these errors can also occur in one-person operation where the total station is remote controlled by a field controller (cf. Leica, 2010a).

Wrongly entered reflector pole heights can hardly be detected in the post processing done in the office. For standard poles, the heights can reach values from 1.3 m to 2.15 m which would result in a maximum height error of ±85 cm. Since negative heights and heights larger than 2.15 m may be set in the total station's user interface, height errors much larger than ±85 cm can occur. These errors can distort height models as needed for high water simulations or other critical applications.

To date, no automated system for measuring the reflector pole height is available.

1.2 Implementation concept

For the verification of the reflector pole heights, the idea is to have a system continuously running in the background. This system calculates the reflector pole height automatically

and informs the user if the calculated height differs significantly from the currently set height at the total station.

Figure 1-1 depicts the basic principle of the height determination. Additionally to the prism on top of the reflector pole (target 1), a second target marking (target 2) is mounted on the fixed part of the pole so that its height above ground level (h_{constant}) is constant for every reflector pole height. Thus, it is not needed to measure the whole reflector pole height but only the variable height between target 1 and 2 (h_{variable}). With knowledge of the constant height of target 2, the height of target 1 above ground level is computed by

$$h = h_{\text{variable}} + h_{\text{constant}}. \tag{1-1}$$

The zenith angle (V_1) and the slope distance (d_1) to target 1 are known from the polar measurement executed by the user. Measuring the angle between target 1 and 2 (α) yields the zenith angle to target 2 ($V_2 = V_1 + \alpha$). With those measurements and the assumption of a vertical orientation of the reflector pole, the height between target 1 and 2 may be computed from

$$h_{\text{variable}} = d_1 \frac{\sin \alpha}{\sin V_2}. \tag{1-2}$$

For the measurement of the angle α, two different sensors of the total station are used in this thesis: its automatic target recognition (ATR, cf. sections 3 and 5.1) and its wide-angle camera (WAC, cf. sections 4 and 5.2).

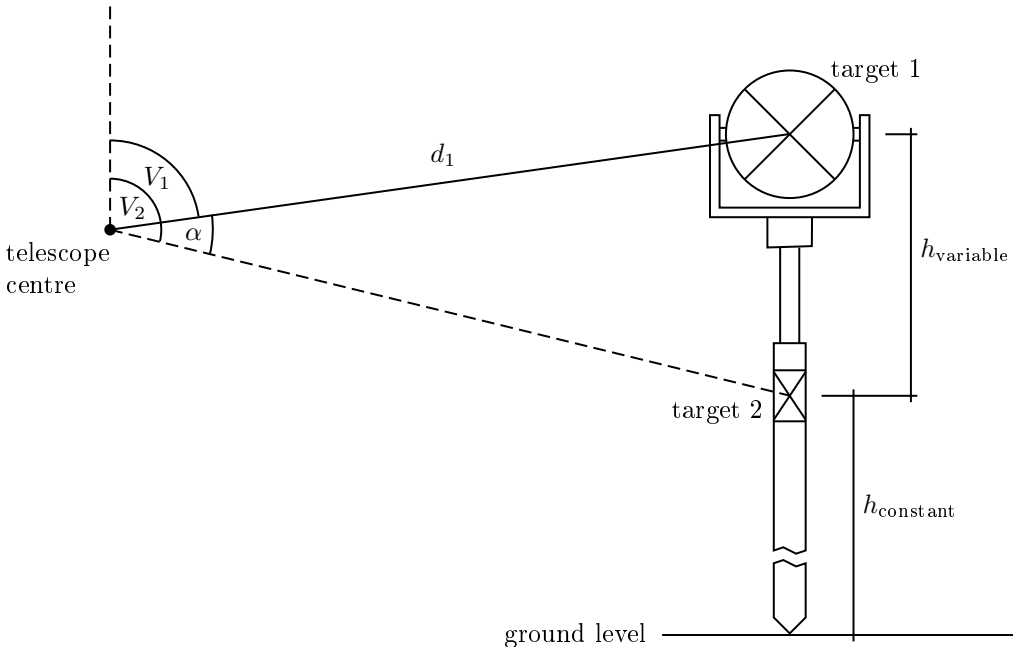

Figure 1-1: Basic principle of the height determination

In the proposed method, the necessary measurements for the automated calculation of the reflector pole height are entirely left to the total station. Thus, the reflector pole does not need to be equipped with sensors (e.g. a laser distance meter) or radio communication facilities for measuring the height and transferring it to the total station. Another important property of the system is, that after positioning the telescope onto the prism (target 1), which is necessary for polar measurements, no additional moving of the telescope is required for measuring the reflector pole height. This enables a fast height measurement without changing the workflow of the user.

1.3 Prototype

To test the achievable accuracy and the operating range of the developed system for the automated reflector pole height verification, a prototype was assembled (figure 1-2).

Therefore, a standard reflector pole (Leica GLS11 Telescopic Pole, extendible from 1.3 m to 2.15 m) was modified by mounting an auxiliary prism (Leica circular prism GPR1) and a fiducial marker (size: 8×8 cm, border width: 1 cm) on the fixed part of the pole. The main prism (GPR1), which is used as the actual target in polar measurements, remains unchanged, i.e. it is mounted on the flexible part of the pole.

Figure 1-2: Prototype of the modified reflector pole

The auxiliary prism is used as the additional target marking in the ATR-based method of the height verification (cf. sections 3 and 5.1) where the fiducial marker is used in the WAC-based method (cf. sections 4 and 5.2).

Table 1-1 shows the separations between the main prism and the additional target markings for the developed prototype. These values are important for the operating range of the system described in this thesis (cf. section 5.3). The heights of the auxiliary prism and the fiducial marker above ground level are constant since they are mounted on the fixed part of the pole (cf. figure 1-1).

Table 1-1: Separations between the main prism and the additional target markings for different reflector pole heights (RPH) and constant heights above ground level

method	1.3 m RPH [m]	2.15 m RPH [m]	height above ground level [m]
ATR	0.27	1.12	1.03
WAC	0.37	1.22	0.93

As mentioned in section 1.4, the system does not account for any tilt of the reflector pole. Using the prototype depicted in figure 1-2, only tilts orthogonal to the sighting could be detected (by comparing the horizontal and the vertical angle between the main prism and the auxiliary prism or the fiducial marker). Since the effect of a tilt of the reflector pole on its height is very small (cf. section 1.4), the measurable tilt is not considered.

Due to the provisional assembling of the prototype, the auxiliary prism and the fiducial marker show offsets to the main prism's vertical axis. These offsets need to be accounted for an accurate determination of the reflector pole height (cf. section 2).

1.4 Aspired accuracy and limitations of the system

Most reflector poles are graduated in centimetres or 0.05 ft and surveyors typically use reflector pole heights of full centimetres or 0.05 ft. In fact, many surveyors only use heights to the nearest 5 cm (or even to the nearest 10 cm) to facilitate the communication (using a radio connection) between the observer and the assistant. Accordingly, an accuracy of 1 cm for the automated reflector pole height verification is sufficient. Furthermore, the described system does not aim to substitute the manual reading of reflector pole heights but is meant as an augmentation system which alerts when using wrong heights.

As mentioned in section 1.2, a vertical orientation of the reflector pole is stipulated for the automated height verification. The accuracy of the circular level of the used reflector pole is specified with $8'/2\,\text{mm}$. This means that a tilt of the reflector pole of $8'$ (from the plumb line) causes the bubble of the circular level to move for 2 mm from its centre position (Nindl, 2010). Having the bubble within these 2 mm is not too hard to achieve. For the maximum reflector pole height of 2.15 m, a tilt of $8'$ results in a horizontal error of 5 mm where the height error only amounts to 6 μm. Accordingly, a tilt of the reflector pole may be neglected for the automated verification of its height.

The main limitation of the system is the necessity of an unobstructed sighting not only to the prism on top of the reflector pole but additionally to the used target marking mounted on the fixed part of the pole (cf. figure 1-1). In cases of obstructed sightings to the additional target marking, no height verification is possible. However, in these cases the system can still inform the observer to draw special attention to the set reflector pole height.

1.5 Used instrumentation and software

For the investigations, Leica's total station TS15 I 1 R1000 was used. The abbreviations after the name *TS15* (which denotes the series) characterize some of the instruments specifications. The built-in wide-angle camera is marked by the *I* and *1* specifies the accuracy

for angle measurements (1″). The capability of reflectorless distance measurements up to 1000 m is indicated by *R1000*. Table 1-2 provides general informations on the used total station. Detailed informations on the ATR module and the wide-angle camera are given in sections 3 and 4.

The total station's sensor functions were accessed using a serial port connection and the GeoCOM interface. Most of the used GeoCOM commands can be found in Leica (2010b). Some of the used commands are not publicly available and were provided by Leica Geosystems AG for the investigations described in this thesis.

The processing of the measured data was done using MATLAB (v7). For the detection of the fiducial marker, two open source libraries, ARToolKitPlus (v2.1.2) and OpenCV (v2.4.1) were used (both written in C/C++). A short introduction to these libraries is given in section 4.3. The development of the routines was done under Linux Mint 12. After slight modifications, they should be portable to Microsoft Windows or Mac OS.

Table 1-2: General informations on the used Leica TS15 I 1 R1000

Serial number	1613987
Accuracies[1]	
Angular measurement	1″ (0.3 mgon)
Distance measurement[2]	1 mm + 1.5 ppm
Software versions	
SmartWorx	v4.0, build: 2361
BSP[3]	v4.0, build: 748
Sensorboard	v1.19, build: 754
Camera	v1.1, build: 123

[1] Leica (2010c)

[2] standard measurement mode to circular prism GPR1

[3] Board Support Package (operating system)

2 Operating principle of the height determination

Figure 2-1 depicts a flowchart of the developed system for the automated identification of a wrong reflector pole height.

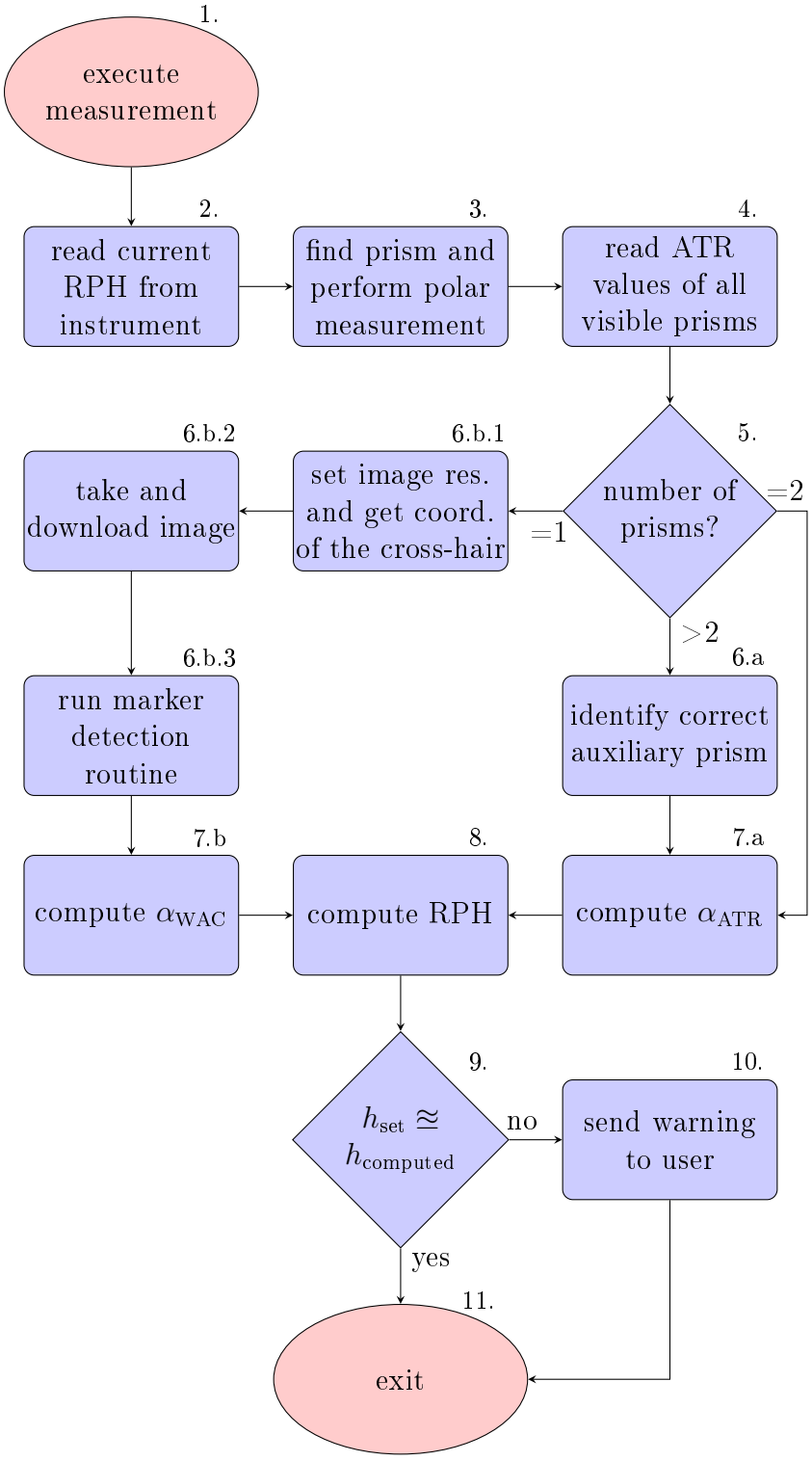

Figure 2-1: Flowchart of the system to identify a wrong reflector pole height (RPH)

1. A polar measurement is executed by the user.
2. After reading the currently set reflector pole height at the total station,
3. the main prism is found automatically (using the ATR module, cf. section 3) and a polar measurement is executed. If the surveyor performs continuous measurements, the instrument may already be locked onto the prism. Of course, the reflector pole height is only necessary/possible to be computed for successful polar measurements.
4. Afterwards, the ATR values of all prisms within the ATR module's usable field of view (cf. section 3.11) are read (using a confidential GeoCOM command).
5. If only one prism is found (i.e. the main prism), the reflector pole height may possibly still be computed by using the wide-angle camera (6.b and 7.b) due to its larger field of view (cf. section 4.1). If more prisms are found, the height can be computed using the ATR module (6.a and 7.a). In a market-ready system, the wide-angle camera could as well be used for cases where the ATR-based method works. This is not done for the prototype (the reason is given in 6.b.2).
6. Dependent on the used method, processes for the computation of the angle between the main prism and the auxiliary prism (ATR-based, 6.a) or the fiducial marker (WAC-based, 6.b.1 and 6.b.2) are made.

6.a For the ATR-based method, the correct auxiliary prism (if more than two prisms were found) is determined by investigating the horizontal ATR values. Since the telescope is positioned onto the main prism and the reflector pole is assumed to be levelled (cf. section 1.4), the prism with the smallest horizontal ATR value may be regarded as the correct auxiliary prism.

6.b.1 For the WAC-based method, the pixel coordinates of the telescope's cross-hair are determined using the GeoCOM command `OVC_GetActCameraCentre` (Leica, 2010b, p. 101) which is a function of the image resolution and the slope distance. In the test measurements (cf. section 5.2), the highest image resolution (2560×1920 pixel) was used.

6.b.2 After taking the image it is downloaded via a serial port connection. For the highest image resolution, this takes over 2 minutes. Thus, the WAC-based method is only used if the ATR-based method does not work.

6.b.3 In the downloaded image, the fiducial marker is detected using the routine described in section 4.3.

7. The computation of the angle between the main prism and the auxiliary prism (α_{ATR}, 7.a) or the fiducial marker (α_{WAC}, 7.b) depends on the used method. Details are depicted in figure 2-2.

8. Corresponding to the used method, the separation between the main prism and the auxiliary prism or the fiducial marker is computed (cf. figure 2-3). Adding the constant height of the auxiliary prism or the marker to this separation yields the height of the main prism above ground level, i.e. the reflector pole height.

9. The difference between the currently set and the computed height is calculated.

10. If this difference is outside a specified tolerance, the user is alerted that a wrong reflector pole height is set.

11. Otherwise, the measured data is stored as normal.

Figure 2-2 derives the computation of the angle between the main prism and the auxiliary prism (α_{ATR}) or the fiducial marker (α_{WAC}).

For the ATR based method, the angle is computed by

$$\alpha_{\mathrm{ATR}} = V_2 - V_1 \tag{2-1}$$

where V_1 and V_2 are the vertical ATR corrections of the main and the auxiliary prism, respectively.

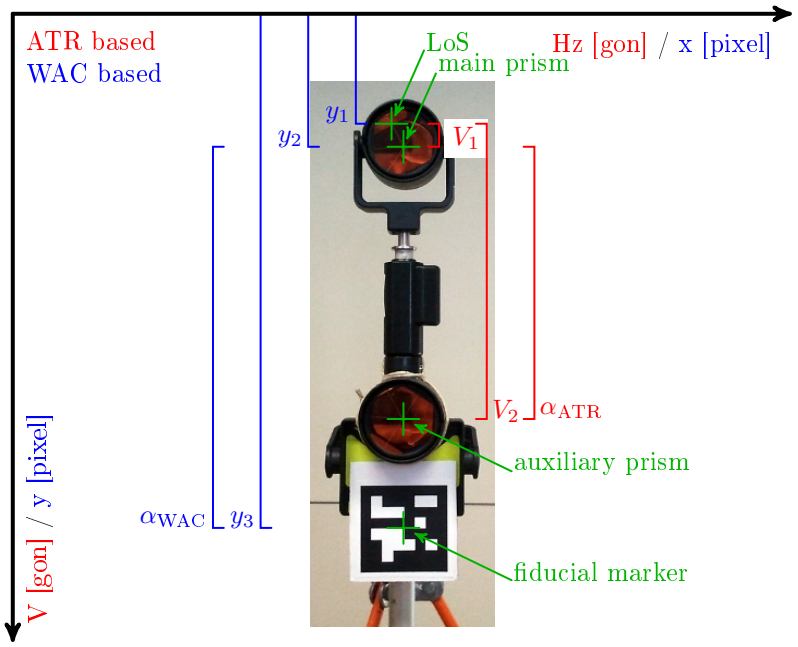

Figure 2-2: Computation of the angle between the main prism and the auxiliary prism (red) or the fiducial marker (blue)

For the WAC-based method, the angle results from

$$\alpha_{\mathrm{WAC}} = \omega\,(y_3 - y_2) \tag{2-2}$$

where ω is the vertical field of view of a single pixel (gon/pixel) and y_2 and y_3 denote the vertical image coordinates (in pixel) of the main prism and the fiducial marker, respectively. The GeoCOM command `OVC_GetActCameraCentre` (Leica, 2010b, p. 101) returns the image coordinates of the telescope's line of sight (y_1). The vertical image coordinate of the main prism is gained from

$$y_2 = y_1 + V_1/\omega. \tag{2-3}$$

The vertical field of view of a single pixel (ω) may be computed by relating the vertical field of view of the wide-angle camera (gained from GeoCOM command `GetCameraFoV`, cf. Leica, 2010b, p. 98) to the number of vertical pixel (1920 for the maximum resolution, cf. Leica, 2010c) which resulted in $\omega = 6.80\,\mathrm{mgon/pixel}$.

The computation of the separation between the main prism and the fiducial marker is depicted in figure 2-3. Due to an offset between the centres of the telescope and the camera, the computation of the height using the WAC-based method is slightly more complicated than using the ATR-based method. The offset between the two centres may be computed from the GeoCOM command `GetCamPos` (Leica, 2010b, p. 96). When positioning the telescope to $Hz = 0\,\mathrm{gon}$ and $V = 100\,\mathrm{gon}$, the resulting offsets in north and height (in the telescope's coordinate system) correspond to the shifts of the camera in direction of the

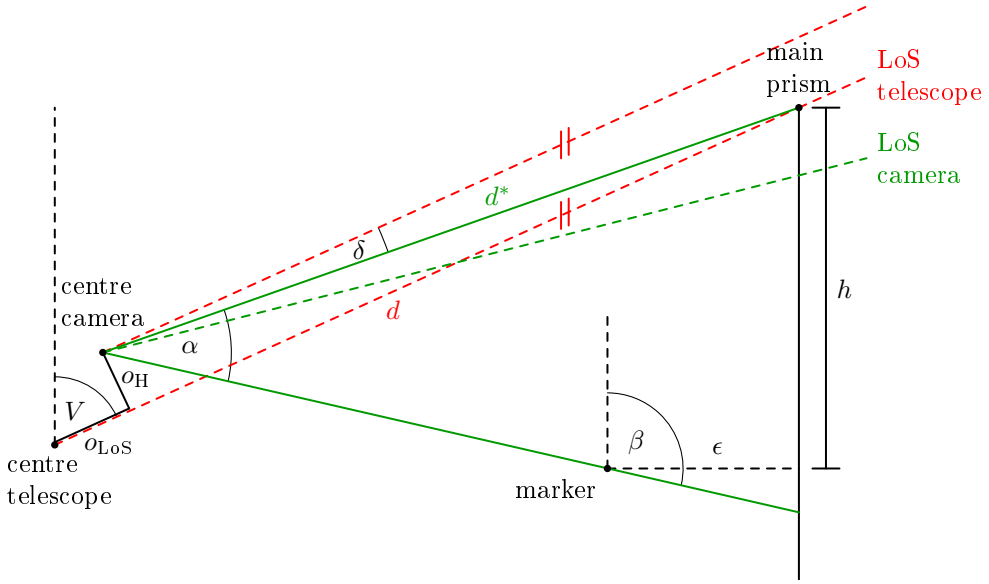

Figure 2-3: Geometry for the reflector pole height determination using the wide-angle camera (not to scale)

telescope's line of sight (o_{LoS}) and orthogonal to it (o_{H}). As an alternative to turning the telescope to a certain position, the gained offsets can be transformed by using Hz and V as rotation angles. The shifts of the camera centre w.r.t. the centre of the telescope were determined to $o_{\mathrm{LoS}} = 60.7\,\mathrm{mm}$ and $o_{\mathrm{H}} = 55.9\,\mathrm{mm}$.

Investigating the image coordinates of the main prism (especially at long distances) shows, that the optical axes of the telescope and the camera are not parallel. However, this is automatically considered when reading the main prism's image coordinates via `OVC_GetActCameraCentre` (Leica, 2010b, p. 101).

For the WAC-based method, the separation between the main prism and the fiducial marker is computed from

$$h = d^* \frac{\sin\alpha}{\sin\beta} + \epsilon \cot\beta \tag{2-4}$$

where α is taken from eq. 2-2 and the distance from the camera's centre to the main prism is computed from the measured slope distance (centre of the telescope - main prism) so that

$$d^* = \sqrt{o_{\mathrm{H}}^2 + (d - o_{\mathrm{LoS}})^2}. \tag{2-5}$$

The angle β results from

$$\beta = V + \alpha + \delta \tag{2-6}$$

where

$$\delta = \tan^{-1}\frac{o_{\mathrm{H}}}{d - o_{\mathrm{LoS}}}. \tag{2-7}$$

The marker's orthogonal offset ϵ from the vertical defined by the main prism has to be taken into account for the prototype described in section 1.3 ($\epsilon = 40\,\mathrm{mm}$).

Using the ATR-based method, α occurs between the lines defined by telescope centre - main prism and telescope centre - auxiliary prism. For the computation of the separation between the main and the auxiliary prism, eq. 2-4 holds with some simplifications. The measured slope distance is introduced directly ($d^* \doteq d$) and $\beta = V + \alpha$ where α is taken from eq. 2-1. For the used prototype, the auxiliary prism's offset ($\epsilon = 39\,\mathrm{mm}$) has again to be taken into account.

3 Investigations on the ATR module

The automatic target recognition (ATR) module is a "device for the rapid detection of the position of a target marking" (Bayer et al., 2000). Today, an automated fine aiming module like the ATR module is part of almost every motorized theodolite with the capability of electronic distance measurement (EDM). These instruments are commonly referred to as automated or robotic total stations. The ATR module's output are the horizontal and vertical angle deviations of the telescope's optical axis from the prism centre. These deviations (or corrections) may be used to position the total station's cross-hair onto the prism centre automatically (motorization required) or to correct the measured horizontal and vertical angle in order to get the precise direction to the prism centre (Bayoud, 2006).

3.1 Operating principle of the Leica ATR module

The basic idea (Bayer et al., 2000; Bayoud, 2006) is to compare two images, where one image is taken while the instrument is emitting an infrared (IR) beam coaxially to the optical axis and the other without this radiation (figure 3-1). Subtracting these two images yields the spot of the prism since other spots (e.g. in figure 3-1 at the car's headlight due to reflections of the sunlight) will cancel out. Furthermore, algorithms for distinguishing between the prism's spot and other spots exist (Leica, 2006; Bayer et al., 2000). The pixel coordinates of the prism spot centre are determined by centroid computations of the row and column wise summations of the light intensities in the difference image (Bayer et al., 2000). In the TS15 instrument, this process is repeated at 37 Hz (Leica, 2010d, p. 126).

(a) IR radiation off (b) IR radiation on

Figure 3-1: Images processed by the ATR module (Bayoud, 2006)

With the knowledge of the pixel size (6 μm, cf. table 3-2) and the focal length (not published), the measured pixel coordinates of the prism spot centre may be related to horizontal and vertical angle corrections (Bayoud, 2007).

The light sensitive element of the ATR module is a 2D array, consisting of complementary metal-oxide-semiconductors (CMOS), which are used for "measuring" the light intensities. In fact, like the charge-coupled device (CCD) technology, CMOS sensors also relate light intensity to electric charge which, after conversion to voltage, is actually measured (for further information see Litwiller, 2001). The advantages of CMOS sensors are sharper images with higher resolution combined with faster image processing (Bayoud, 2007; Litwiller, 2001).

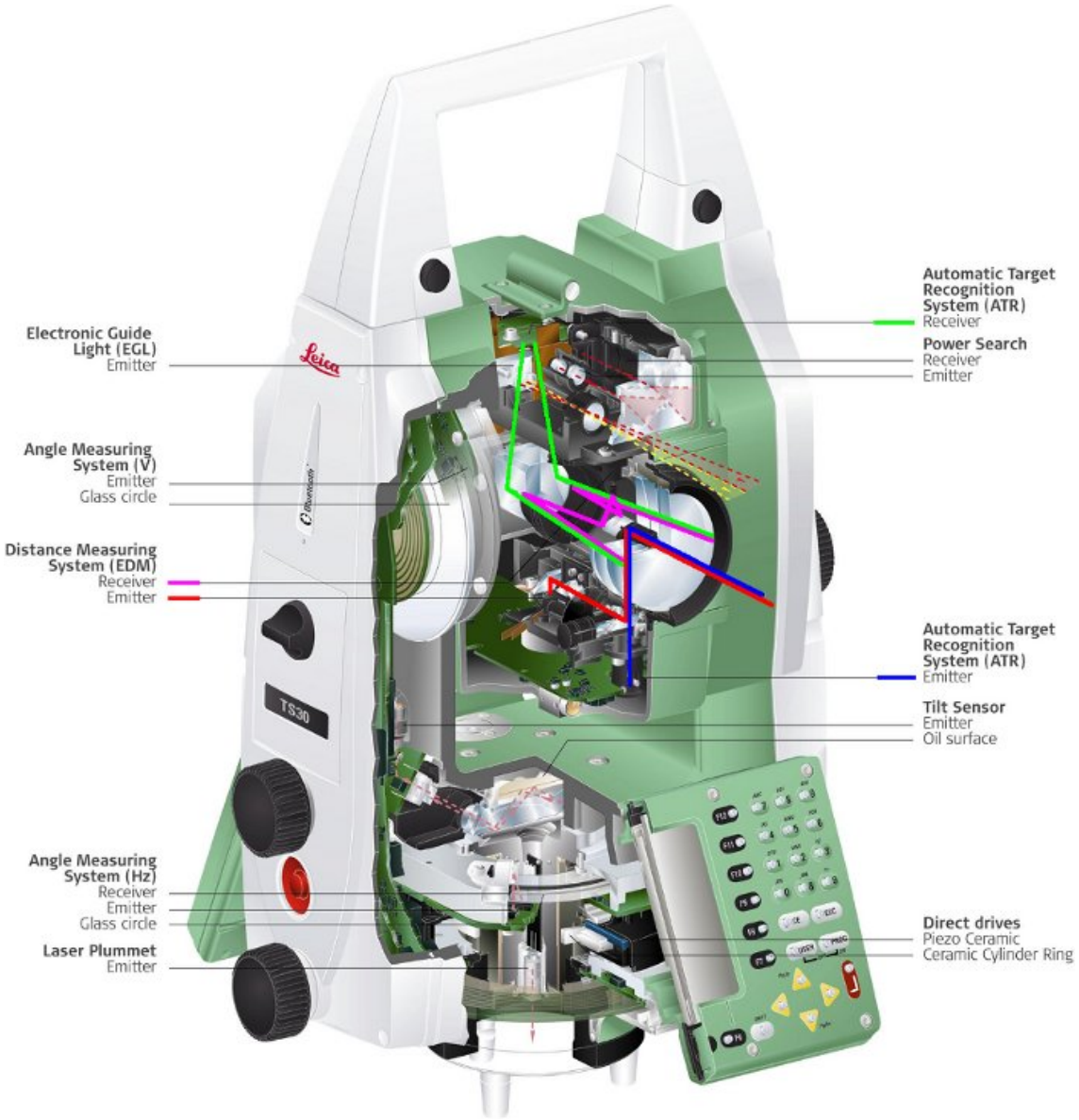

Figure 3-2: Cross-sectional drawing of the Leica TS30 (Zogg et al., 2009, slightly modified)

Table 3-1: Comparison between ATR, EDM and EDM reflectorless (RL) signals of the Leica TS15 (Leica, 2010d, pp. 119-126)

	ATR	EDM	EDM RL
maximum radiant power	10 mW	0.33 mW	5 mW
pulse duration	11 ms	800 ps	
pulse repetition frequency	37 Hz	100-150 MHz	
wavelength	785 nm	650-690 nm	

As pointed out by Bayer et al. (2000), the focus of the ATR module's imaging sensor is constant since the determination of the prism spot centre via centroid computations yields accurate results even for blurred images.

Figure 3-2 shows a cross-sectional drawing of the Leica TS30. Although this is not the instrument used in this thesis (cf. section 1.5), the figure is sufficient to illustrate the optical path of the ATR module's IR beam which is identical to the Leica TS15. The optical path of the EDM module's laser beam is accented since it is emitted coaxially to the IR beam of the ATR module.

The emitted beams are both reflected by a prism and received by the instrument. In the case of the EDM, measurements without reflectors are possible as well. Using the different wavelengths of the beams, i.e. 785 nm for the ATR and 650-690 nm for the EDM (cf. table 3-1), the received signals are directed to different processing units.

Since only one emitter is used for reflector and reflectorless distance measurements (note the common properties in table 3-1), the EDM module has to regulate the intensities of the emitted signal according to the measurement mode (Bayoud, 2007). This is necessary because the radiant power of a reflectorless signal is about 15 times higher than the power of a signal used for reflector measurements (cf. table 3-1) and the reflected signal strength of a reflectorless measurement onto a prism might damage the processing unit.

At this point, it is referred to Bayoud (2006, 2007) and Lienhart et al. (2009) for further information on the electronic distance measurement of Leica instruments. Joeckel et al. (2008) discuss the electronic distance measurement, being focused on other fields of application as well (e.g. laser scanning, satellite measurements), more generally.

3.2 Specifications of the ATR module

Table 3-2 summarizes the characteristics of the ATR module installed in the Leica TS15 as they can be found in present literature.

Operating range The operating range (maximum and minimum range) depends on the measurement mode (ATR or LOCK) and on the prism type. Using small and 360° prisms

Table 3-2: Specifications of the ATR module of the Leica TS15

max. range (ATR/LOCK)[1]	circular prism (GPR1)	1000/800 m
	360° prism (GRZ4, GRZ122)	800/600 m
	mini prism (GMP101)	500/400 m
	360° mini prism (GRZ101)	350/300 m
	reflector tape (60 × 60 mm)	55/- m
min. range[1]	360° prism (ATR/LOCK)	1.5/5 m
max. speed (LOCK)[1]	tangential	5 m/s at 20 m, 25 m/s at 100 m
	radial	5 m/s
prism search[1]	field of view (FoV)	1°25′
	typical search time in FoV	1.5 s
accuracy	base position (GPR1/GMP101/ GRZ122/GRZ4)[1]	1/1/2.3/5 mm
	angle within 5 mgon separation[2]	1″
	angle within 40 mgon separation[2]	2-3″
IR beam[3]	maximum radiant power	10 mW
	pulse duration	11 ms
	pulse repetition frequency	37 Hz
	wavelength	785 nm
light sensitive array[2]	technology	2D complementary metal-oxide-semiconductor (CMOS)
	pixel size	6 μm
	precision of pixel measurement	0.1 pixel

[1]Leica (2010d, pp. 154-157)
[2]Bayoud (2007)
[3]Leica (2010d, p. 126)

limits the maximum range since less IR radiation is reflected compared to a standard circular prism due to a smaller size and/or a weaker reflexivity of the prism.

Compared to the standard measurement mode (ATR), the maximum range in tracking mode (LOCK) is about 1/4 shorter. This results from the operating principle of the ATR module (cf. section 3.1). To determine the spot of a prism on the CMOS array, at least one image must be taken while receiving backscatter of the emitted IR beam. At large distances, attenuation of the emitted signal and interfering light decrease the probability of getting such an image. Since the prism is moving in tracking mode, there is less time to wait for an appropriate backscatter which reduces the maximum range.

Poor conditions (e.g. rain, snow, fog) further lower the maximum ranges (Leica, 2010d, p. 154). The minimum range does not limit the operating range of the system described in this thesis (cf. section 5.3).

Tracking speed The maximum speed, of an object to be tracked, in tangential direction is not limited by the instrument's motorization (45°/s, Leica, 2010c). The velocities 5 m/s

at 20 m and 25 m/s at 100 m both correspond to a rotation velocity of roughly 14°/s which is about 1/3 of the possible value. However, a maximum speed of 18 km/h (=5 m/s) should be sufficient for many purposes (e.g. tracking a prism in one-person operation).

Field of view The field of view, given as a diameter, specifies the separations of the optical axis from the centre of a prism, at which the prism is recognized by the ATR module (i.e. $0.71° = 1°25'/2$).

Accuracy Leica (2010d, pp. 155-157) specifies the accuracy of the ATR measurements with a base positioning accuracy dependent on the prism type. At distances, where the accuracy of the angle measurement (1″) causes an uncertainty above this value, the ATR's accuracy follows the accuracy of the angle measurement. Figure 3-3 depicts the ATR accuracies for a circular prism (GPR1) and a 360° prism (GRZ122).

At distances, where the accuracy of the angular measurement becomes effective, an ATR accuracy of 1″ is only achieved if the separation of the telescope's optical axis from the prism centre is less than 5 mgon. For separations within 40 mgon, accuracies of 2-3″ are to be expected (for further information see Bayoud, 2007).

Using 360° prisms, Favre and Hennes (2000) show that errors up to several millimetres, dependent on the horizontal and vertical orientation of the prism as well as on the distance, occur. This issue is also discussed by Stempfhuber and Kirschner (2008). Therefore, the base position accuracy of a 360° prism, compared to a circular prism, is specified to be lower. Since these errors are beneath the aspired accuracy (1 cm, cf. section 1.4) of the system described in this thesis, they are neglected.

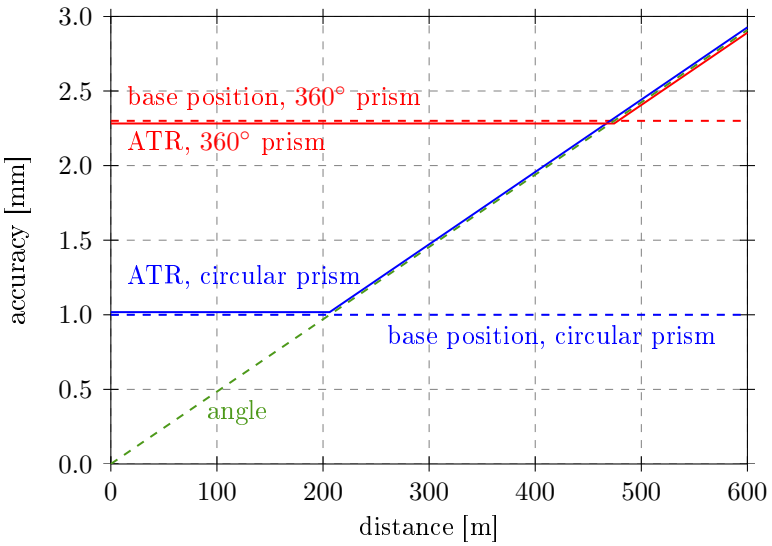

Figure 3-3: Base positioning and ATR accuracies according to Leica (2010d, p. 156)

Emitter unit The emitted signal is located in the near-infrared domain which means that it is invisible to the human eye. Observing the same area as the ATR module through a camera without IR filter (e.g. most smartphone cameras) reveals the spot of the emitted signal (used in sections 3.7 and 3.8.2).

Receiver unit Compared to the wide-angle camera's CMOS array (cf. section 4.1), the ATR module's CMOS array misses two specifications. First, the number of horizontal and vertical pixel and second, the field of view of a single pixel. These two specifications are determined in section 3.8.

3.3 Adopting the ATR module to determine the reflector pole height

The automatic detection of a prism by the ATR module, as described in sections 3.1 and 3.2, can also work for more than one prism, i.e. the angle corrections from the optical axis to several prisms may be read at the same time. This is exactly what is necessary to determine the height of a modified reflector pole without aiming at the auxiliary prism directly (cf. section 1.3 for the assembling of the modified reflector pole). The procedure is to measure the distance and the angles to the main prism, at which the telescope points. Reading the ATR corrections of the auxiliary prism, while still aiming at the main prism, yields the angle between the two prisms which is used in eq. 2-4 to compute the reflector pole height. Compared to the impractical method of performing polar measurements to both prisms, this method is much faster since the telescope does not need to be moved. However, the GeoCOM commands for reading the ATR corrections are not published in Leica (2010b) since they are classified as confidential.

The spot of the main prism will always be located close to the principal point of the CMOS array since the telescope aims at this prism. This is the standard configuration for total station-based measurements and the specifications of section 3.2 concerning accuracies should hold. These accuracies are absolutely sufficient for the aspired accuracy (1 cm, cf. section 1.4) of the system described in this thesis. On the contrary, the spot of the auxiliary prism will be located near the lower boundary area of the CMOS array where no accuracies are specified by the manufacturer. For separations within 40 mgon between the optical axis and the prism centre, Bayoud (2007) specifies the accuracy with 2-3″. At a distance of 100 m, the 40 mgon result in a possible separation of 63 mm between the centres of the main and the auxiliary prism. Regarding the diameter of a circular prism (62 mm, Mao and Nindl, 2009) and the limited operating range, this is not practical. Since the measurements outside the 40 mgon separation may be degraded in a presently unpublished amount, the following issues are investigated in sections 3.9 and 3.10:

- usable field of view of the ATR module
- accuracies of the ATR values within the usable field of view
- dependence of the accuracies on the prism type (circular prism and 360° prism)
- separability of two prisms, located next to each other, at long distances

3.4 Implementation of the test routine

To determine the errors of the ATR module, a MATLAB routine was developed. The basic idea is to perform angle measurements at different separations of the optical axis from the prism centre and to compare them to the respective corrections of the ATR module. The ATR values are read using a confidential GeoCOM command provided by Leica Geosystems AG, which reads the ATR values of several prisms. Each output value was set to consist of 25 ATR measurements. The functioning of the routine is illustrated in figure 3-4.

1. A user action is needed at the very beginning of the test procedure. After setting the extension w.r.t. the prism centre and the resolution of the area to be tested (1.a), the telescope's cross-hair is manually positioned onto the prism centre (1.b).

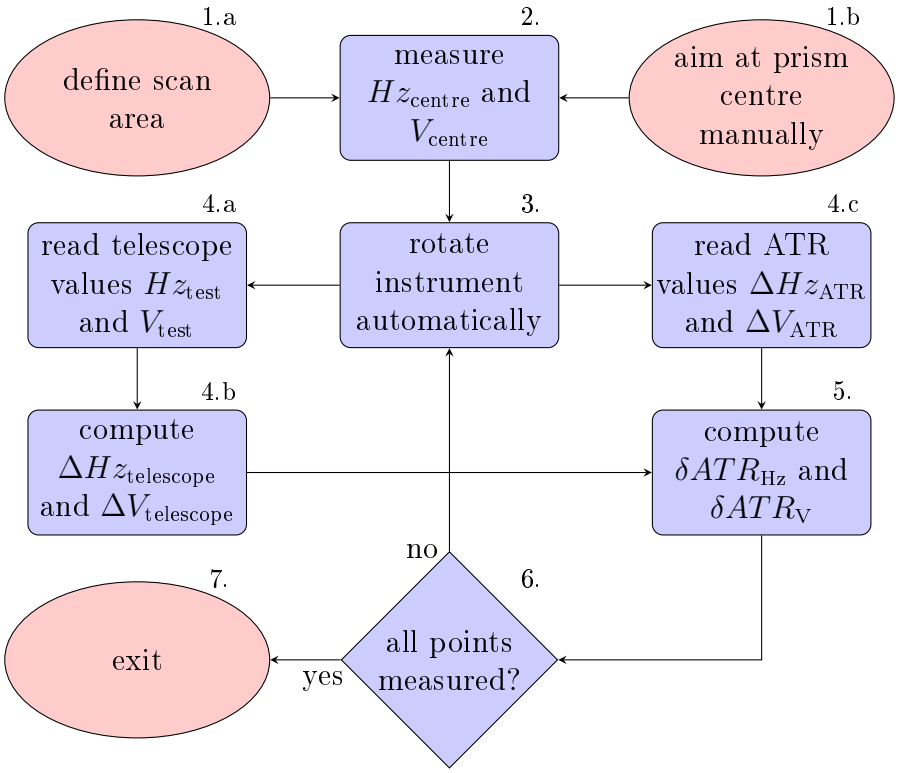

Figure 3-4: Flowchart of the ATR test routine

2. At this centre position, the telescope's angles Hz_{centre} and V_{centre} as well as the ATR values are read. Depending on the settings, prior to the initial measurements an ATR and/or a wide-angle image is taken for visualization purposes. ATR and WAC images can be captured using the GeoCOM commands `TakeTccImage` (Leica, 2010b, p. 146) and `TakeImage` (Leica, 2010b, p. 100) where WAC images can also be captured with the total station's on-board software.

3. The instrument is moved automatically to the next point specified by 1.a.

4. There, the telescope's angles Hz_{test} and V_{test} are read (4.a). The separations of the optical axis from the prism centre are computed (4.b) according to

$$\Delta Hz_{\text{telescope}} = Hz_{\text{centre}} - Hz_{\text{test}} \tag{3-1}$$

$$\Delta V_{\text{telescope}} = V_{\text{centre}} - V_{\text{test}} \tag{3-2}$$

   The ATR values ΔHz_{ATR} and ΔV_{ATR} are promptly read (4.c) after the angle measurement without moving the instrument. If no ATR measurement is possible, the respective point is appropriately marked.

5. The ATR errors are computed by comparing the ATR values to the reference values obtained by the angle measurements:

$$\delta ATR_{\text{Hz}} = \Delta Hz_{\text{ATR}} - \Delta Hz_{\text{telescope}} \tag{3-3}$$

$$\delta ATR_{\text{V}} = \Delta V_{\text{ATR}} - \Delta V_{\text{telescope}} \tag{3-4}$$

   These errors are a measure for the quality of the ATR values at different separations of the optical axis from the prism centre.

6. Steps 1. to 5. are repeated until all points specified by 1.a are measured.

7. After storing the measured data and writing some statistics to a log file, the procedure is ended.

3.5 Test area and setup

The errors of the ATR module were tested at several distances (cf. figures 3-5 and 3-6) using two different prisms: a Leica circular prism GPR1 and a Leica 360° prism GRZ122 which are in the following briefly denoted as circular prism and 360° prism.

From investigations done by Favre and Hennes (2000) it is known, that errors up to several millimetres can occur for different rotation states of a 360° prism. Thus, different orientations of the 360° prism (cf. figure 3-7) were also investigated.

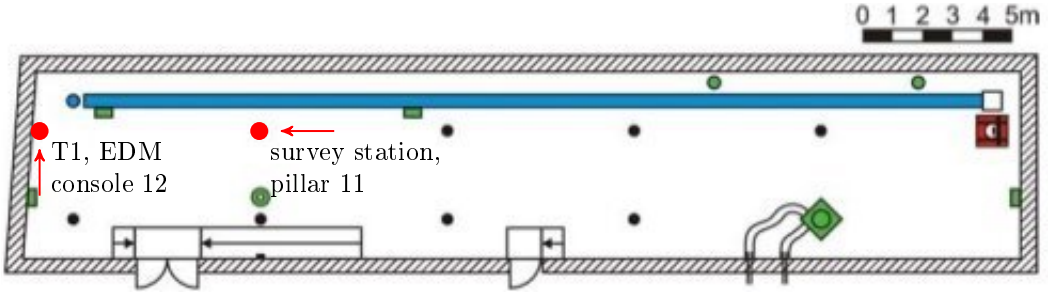

Figure 3-5: Survey station in the Geodetic Metrology Laboratory (Steyrergasse 30), test area with a short (7.6 m to T1) distance (based on Woschitz, 2003, p. 96)

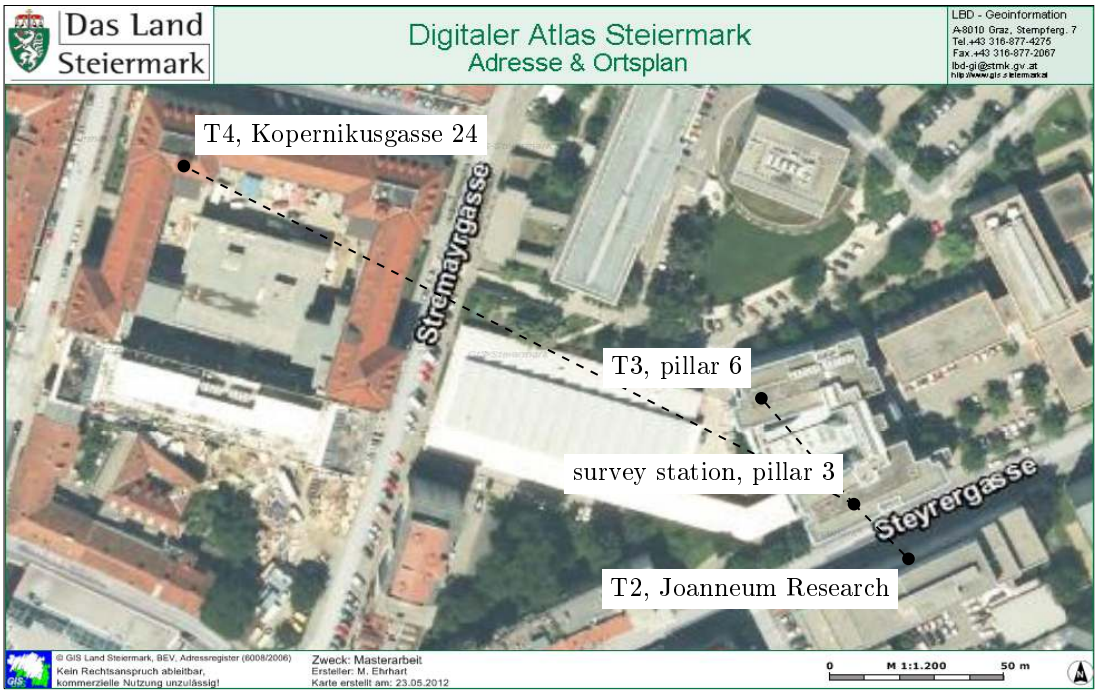

Figure 3-6: Survey station at the roof of the geodesy building (Steyrergasse 30), test area with medium (25.2 m to T2 and 40.0 m to T3) and long (215.2 m to T4) distances (orthophoto source: www.gis.steiermark.at)

The non-rotated state of the 360° prism refers to the position where one of the six triple-prisms is oriented towards the instrument. The rotated state results from a rotation by 45° round the vertical axis so that the edge between two triple-prisms is oriented towards the instrument.

3.6 Errors at the principal point

Dependent on the accuracy, within which the prism centre is sighted, the distance to the target and the adjustment of the ATR module (cf. Leica, 2010d, pp. 79-83), errors (cf. eqs. 3-3 and 3-4) occur at the principal point (figure 3-8a).

(a) non-rotated (b) rotated

Figure 3-7: Different rotation states of the Leica 360° prism GRZ122

Without correction, i.e. subtraction of the ATR values at the principal point from the ATR values at the other points (figure 3-8b), this will falsify the results for the following reason. The zenith angle of the auxiliary prism is computed by adding its vertical ATR value to the zenith angle of the main prism. The received zenith angle is already corrected by the (small) vertical ATR value of the main prism. Hence, adding the measured ATR value of the auxiliary prism will apply this correction twice and will falsify the angle between the two prisms by the ATR value of the main prism. Therefore, the figures in the sequel will show the ATR errors corrected by the error at the principal point.

In the experiments of section 3.9, the errors at the principal point amounted to a few mgon since the prism centre was manually aimed at. However, when observing prisms in tracking mode, separations of the optical axis from the prism centre up to 40 mgon are possible (cf. Bayoud, 2007). In such cases, a twofold appliance of the main prism's ATR correction can cause large errors in the computed separation between two prisms.

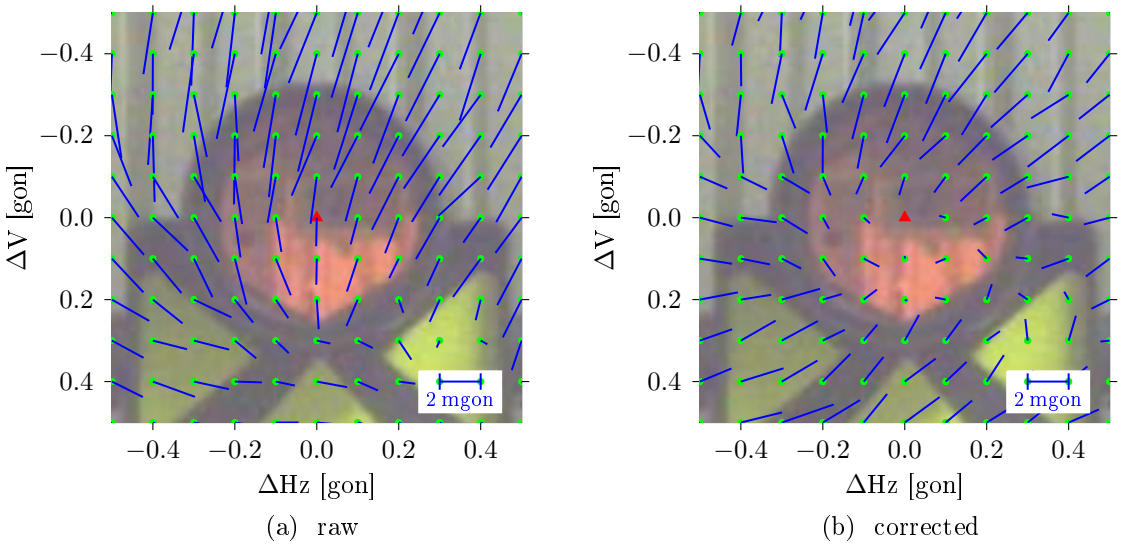

(a) raw (b) corrected

Figure 3-8: ATR errors round the principal point (red triangle)

3.7 Multi-spot issue

Looking at a 360° prism, the eye of the observer will be reflected up to three times (dependent on the horizontal and vertical angle of incidence). Since the automatic target recognition is an image based technique (cf. section 3.1), this issue also occurs here.

This can be illustrated by the following experiment where ATR images were taken (using the GeoCOM command `TakeTccImage`, cf. Leica, 2010b, p. 146) at a distance of 12.6 m. Using the IR beam emitted by the ATR module for visualizing the spots reflected by the prism is not possible since ATR images cannot be manually taken while performing measurements or being in tracking mode (where IR light is emitted). Thus, IR light was emitted into the telescope's ocular using an infrared LED (HIRL5015: $\lambda = 865\,\text{nm}$, radiant intensity 60 mA). Even better results are gained if the ocular is removed for this purpose. The experimental setup is depicted in figure 3-9.

Figure 3-10 shows the spots of a circular prism and a rotated 360° prism (cf. figure 3-7). The two spots being reflected from the 360° prism are clearly visible. The black area at the prism spot centre and the cut at the bottom may be regarded as the shadow of the components, which direct the ATR and the EDM beam into the optical axis of the telescope (cf. figure 3-2).

When reading multiple ATR values (using a GeoCOM command provided by Leica Geosystems AG), one 360° prism is sometimes identified as two separate prisms. This is

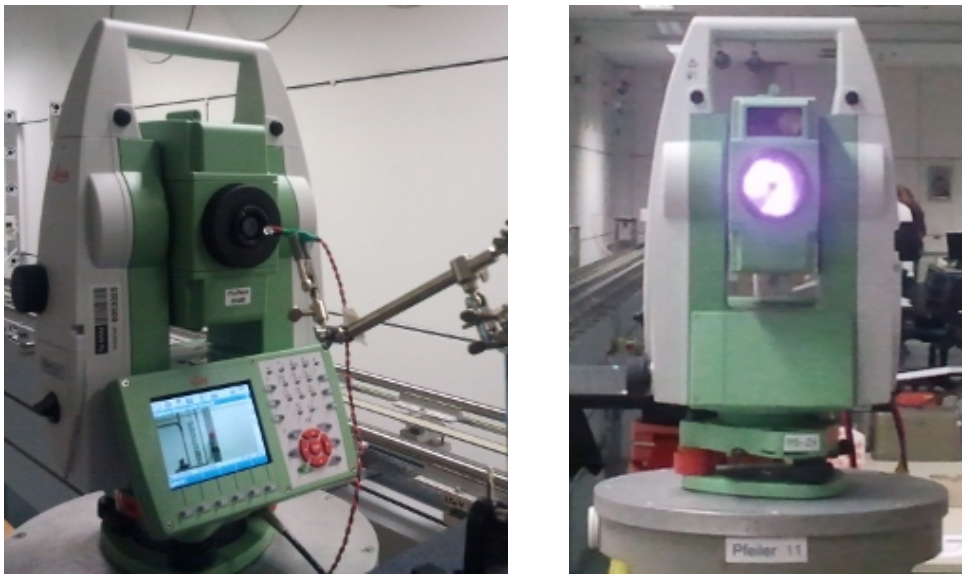

(a) (b)

Figure 3-9: Experimental setup (a) for capturing a prism spot on the ATR module's CMOS array using an external IR source and emitted IR beam (b) captured by a smartphone camera

depicted in figure 3-11a, where “multiple errors” occur for selected points at the boundary area of the field of view although the prism is not rotated (cf. figure 3-7). Simply averaging these errors, as depicted in figure 3-11b, does not correct the effect thoroughly but for clarity, the figures in the sequel will show the averaged errors if necessary. However, in the experiments, the effect only appeared at the boundary area of the field of view, where no useful measurement can be made anyway (cf. sections 3.9.1 and 3.9.2).

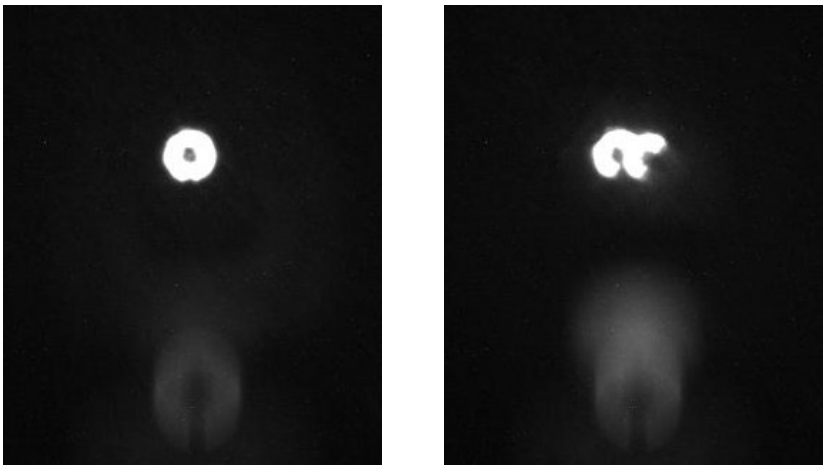

(a) circular prism (b) 360° prism

Figure 3-10: Spots of different prisms on the ATR module’s CMOS array (illuminated by an externally attached IR source)

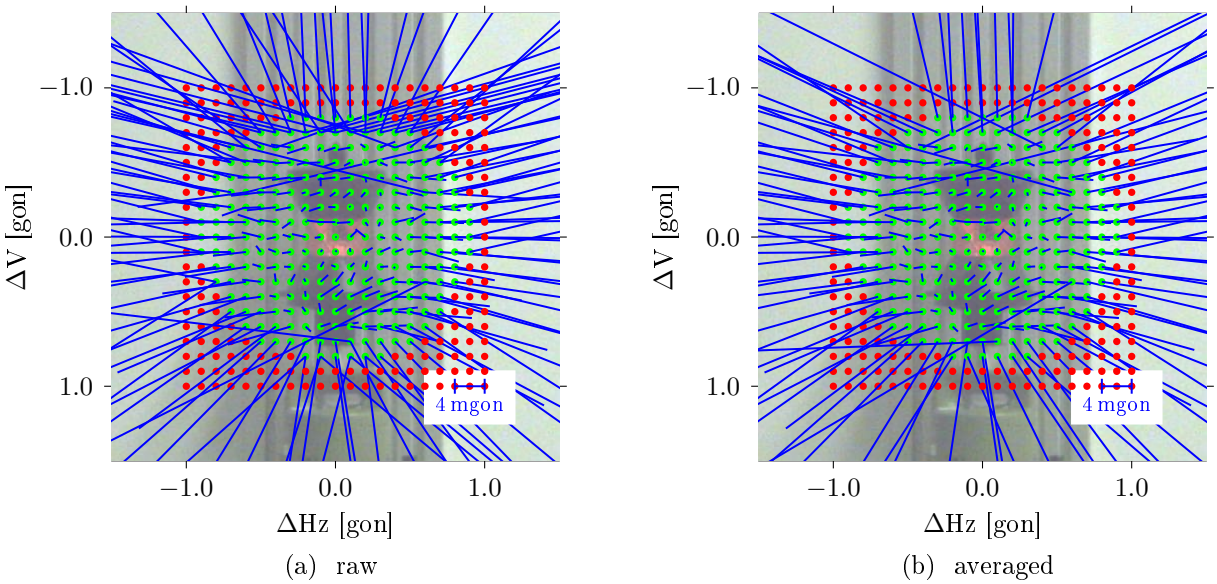

(a) raw (b) averaged

Figure 3-11: Multiple spot detection using a 360° prism

3.8 Verifying the ATR module's field of view

The manufacturer specifies the ATR module's field of view with 1°25′ (given as a diameter, cf. table 3-2). Since the field of view is of major importance for the possible operating range of the ATR-based verification of the reflector pole height, this specification was verified. Therefore, two limiting factors, which are not given by the manufacturer directly, need to be known: the restriction due to the size of the CMOS array and the restriction due to the diameter of the emitted IR beam.

3.8.1 CMOS array

To determine the field of view resulting from the ATR module's CMOS array, the number of horizontal and vertical pixel as well as the field of view of a single pixel (mgon/pixel) need to be known. The number of pixel may be read from the properties of an image captured by the ATR camera (700×480 pixel). To determine the field of view of a single pixel, two GeoCOM commands provided by Leica Geosystems AG were used. For one prism, these commands read the ATR values (gon) and the centre of the prism spot on the CMOS array (pixel), respectively.

Reading the ATR corrections at the points $\Delta Hz = \Delta V = -0.4 : 0.05 : 0.4$ gon (w.r.t. the prism centre) in gon while reading the centres of the prism spots on the CMOS array in pixel, resulted in the almost straight lines depicted in figure 3-12.

The slope k of the straight given by

$$y\ [\text{gon}] = k\ [\text{gon/pixel}] \cdot x\ [\text{pixel}] + d\ [\text{gon}] \tag{3-5}$$

yields the field of view of a single pixel. Since both values y (ATR corrections in gon) and x (prism spot centres in pixel) are measured quantities affected by uncertainties, an

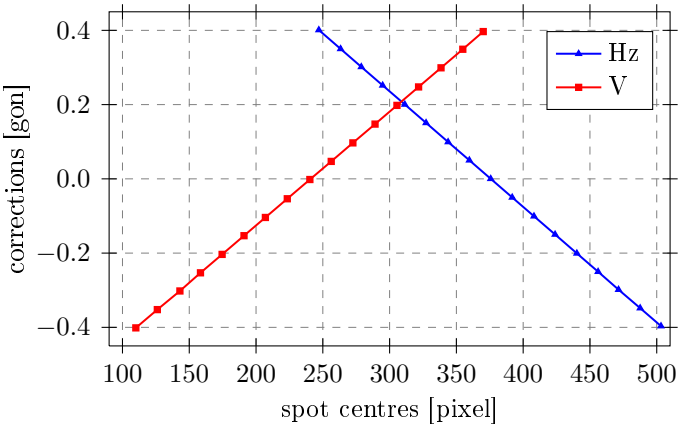

Figure 3-12: ATR corrections and prism spot centres on the CMOS array for corresponding points (horizontal pixel counted from right to left, vertical pixel from top to bottom)

orthogonal regression was chosen to estimate the slopes of the straight lines. The formulae are taken from Niemeier (2008, pp. 399-404). A detailed derivation can also be found there.

First, a matrix

$$\mathbf{X} = [\mathbf{x} - \overline{x}, \mathbf{y} - \overline{y}] \tag{3-6}$$

containing the measurement-tuple (x_i, y_i) reduced by their mean value is set up ($\mathbf{x}$ and $\mathbf{y}$ are column vectors). Now the covariance matrix

$$\mathbf{C} = \mathbf{X}^T\mathbf{X} \tag{3-7}$$

is computed. The slope k is computed from the components of the covariance matrix' eigenvector $\mathbf{v}$ related to the maximum eigenvalue according to

$$k = \frac{v_2}{v_1}. \tag{3-8}$$

Finally, the offset may be computed from

$$d = \overline{y} - k\overline{x}. \tag{3-9}$$

The resulting residuals $\mathbf{r}$ were tested for outliers using the mean-absolute-deviation

$$MAD = \text{median}(|\mathbf{r} - \tilde{r}|). \tag{3-10}$$

The residuals are classified as outliers if

$$|r_i - \tilde{r}| > 3/z_{0.75}\, MAD \tag{3-11}$$

where the factor $1/z_{0.75} = 1.483$ is used to make the MAD an estimate of standard deviation (Ellison et al., 2009, p. 56). The factor 3 provides the usual 3σ-criterion.

After removing the outliers and re-estimation, the slopes of both straight lines (cf. figure 3-12) were determined to 3.1 mgon/pixel. This procedure was done twice gaining identical results. The residuals of the two test series are depicted in figure 3-13.

The estimated value corresponds to the specifications given by the manufacturer (cf. section 3.2): the angle is measured with an accuracy of $1''$ and the pixel on the CMOS array are read to sub-pixel level (Bayoud, 2007). A pixel with a field of view of 3.1 mgon/pixel, read to 0.1 pixel, results in an accuracy of 0.31 mgon which corresponds to roughly $1''$.

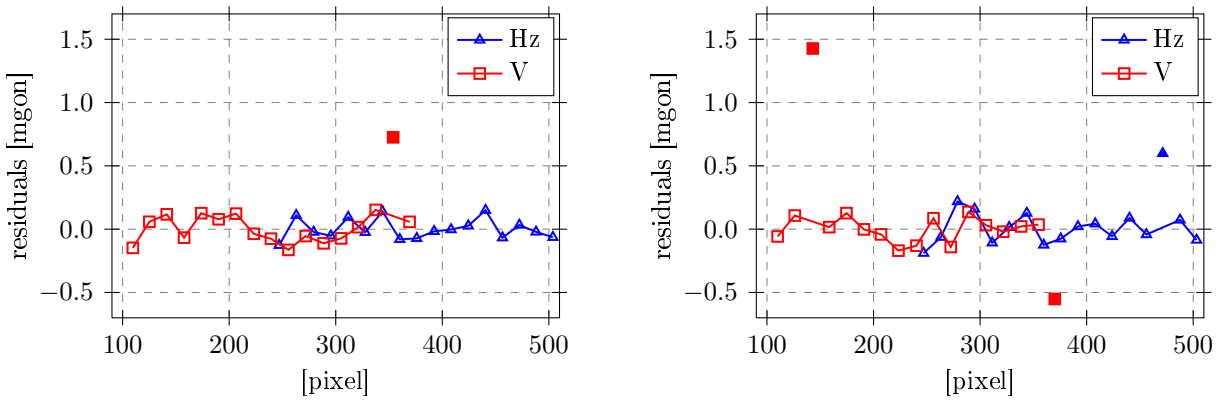

(a) test series #1 (b) test series #2

Figure 3-13: Residuals and outliers for the orthogonal regression

Setting $y = 0$ and rearranging eq. 3-5 to

$$x = -\frac{d}{k} \tag{3-12}$$

yields the position of the optical axis on the CMOS array in pixel. The two test series both result in 375.8 pixel (horizontal, counted from right to left) and 240.9 pixel (vertical, counted from top to bottom). However, these values are subject to change after each adjustment of the ATR module following Leica (2010d, pp. 79-83).

3.8.2 Diameter of the IR beam

The second limiting factor for the ATR module's field of view is the diameter of the emitted IR beam. The setup of the experiment for the determination of this diameter is depicted in figure 3-14a.

The telescope's cross-hair was positioned onto the corner of a square of a gridded paper (zenith angle 100 gon) and a reflectorless distance measurement was executed ($d =$ 2.538 m). Afterwards, repeated ATR measurements were made in order to have IR light emitted by the instrument. At the same time, pictures of the same area as observed by the total station were taken using a webcam with removed IR filter. One of these images is depicted in figure 3-14b.

The radius of the spot is about 6.3 times the edge of one square. Knowing the spacing between the squares (5 mm), the diameter equals 63 mm which results in an angle of 1.422° at a distance of 2.538 m. This corresponds to 1°25.3′ which reproduces the manufacturer's specification of 1°25′ (cf. table 3-2) almost perfectly.

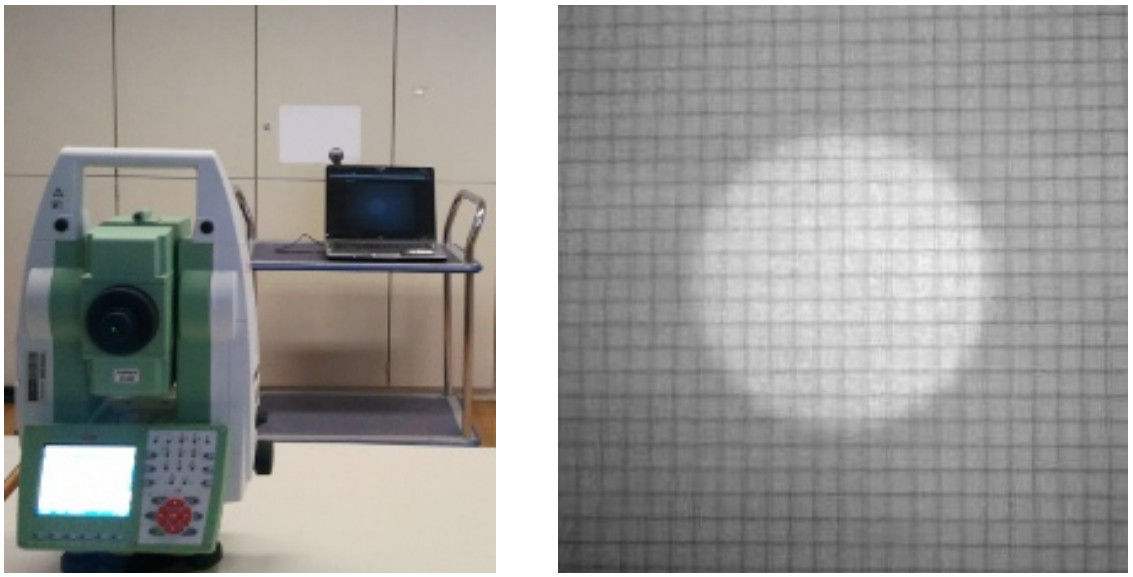

(a) experimental setup (b) observed spot

Figure 3-14: Diameter of the IR beam emitted by the ATR module

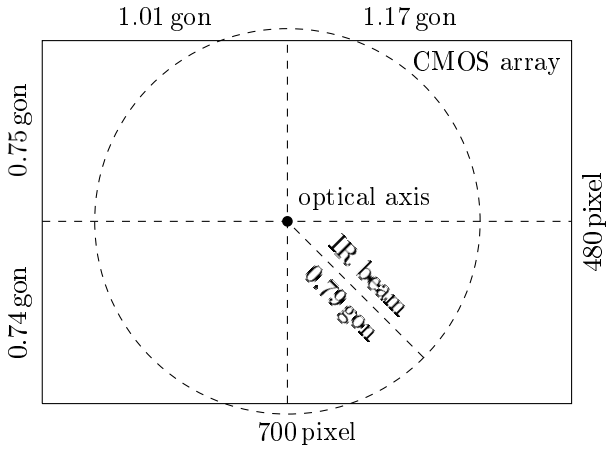

Figure 3-15: Field of view of the ATR module resulting from the CMOS array and the emitted IR beam

3.8.3 Conclusions

A huge CMOS array would be useless if the emitted IR beam had a small diameter (and vice versa) since the ATR module only works if the prism is sufficiently illuminated by the IR beam and if a sufficient large area of the reflected spot is imaged on the CMOS array (cf. section 3.9.4 for a detailed explanation).

Figure 3-15 shows that the CMOS array's size and the diameter of the emitted IR beam are well balanced. Neglecting the small areas at the top and bottom of the IR beam, the ATR module's field of view as given by the manufacturer (1°25′ in diameter, cf. table 3-2) is verified.

3.9 Accuracies of the ATR module

The manufacturer's specification concerning the ATR module's field of view (cf. table 3-2, verified in section 3.8) results in a maximum separation of 0.79 gon between the optical axis and the centre of a prism. Figure 3-16 depicts images taken by the ATR camera for two selected separations. The background stems from a scaled image captured by the wide-angle camera. ATR measurements are possible in both cases since the prism is visible to the ATR module. However, the quality of the ATR measurements for separations larger than 40 mgon (cf. table 3-2) is not specified and needs to be determined in order to use the ATR module for the verification of reflector pole heights (cf. section 3.3).

Therefore, the test routine introduced in section 3.4 was executed in various configurations (distance, prism type, light conditions, orientation of the 360° prism, wrong prism type set at the total station). The maximum separation of the optical axis from the prism centre, in horizontal and vertical direction, was set to ±1 gon. The scan resolution was set to 0.1 gon resulting in 441 (= 21 · 21) measured separations for each run of the test routine.

The results are corrected for the error at the principal point (cf. section 3.6) and multiple spot detections (cf. section 3.7). The test areas are described in section 3.5.

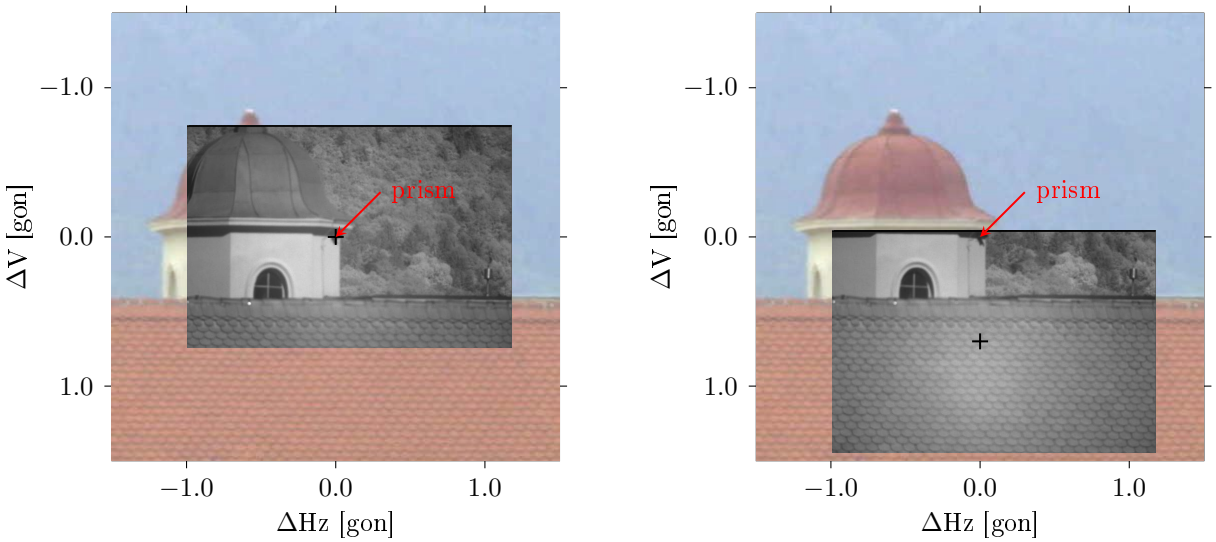

(a) ΔHz = 0, ΔV = 0 (b) ΔHz = 0, ΔV = +0.7

Figure 3-16: ATR images (grey) for different separations of the optical axis from the prism centre

3.9.1 Short distances

For short distances, the ATR errors (expressed in angles) are expected to be large since the base position accuracies of 1 mm and 2.3 mm for circular and 360° prisms (cf. section 3.2) result in large angular errors at short distances. At 7.6 m, these base position accuracies result in 8.4 mgon and 19.3 mgon, respectively.

However, figure 3-17 shows that the errors hardly exceed 3 mgon within a separation of ±0.6 gon when using a circular prism. Figure 3-18 depicts that this also holds true for a non-rotated (cf. figure 3-7) 360° prism when limiting the separations to ±0.5 gon. Figure 3-18 furthermore reveals, that the effect of a wrong prism type in the total station's settings is negligible - at least for the ATR measurements. A wrong prism type of course affects the distance measurements strongly since the additive constants of the different prism types vary by several centimetres (cf. Mao and Nindl, 2009). A rotation of the 360° prism (cf. figure 3-7) changes the pattern of the errors strikingly (compare figures 3-18 and 3-19). The errors start to exceed the 3 mgon for separations larger than 0.3 gon.

The huge (up to 0.16 gon) errors at the boundary area in figures 3-17 to 3-19 are not in contradiction to the manufacturer's specifications (cf. section 3.2). The given accuracies (1″ and 2-3″) are limited to small separations of the optical axis from the prism centre (5 mgon and 40 mgon). If a prism is spotted at a larger separation, the ATR module does not correct the telescope's angle measurements promptly but moves the telescope

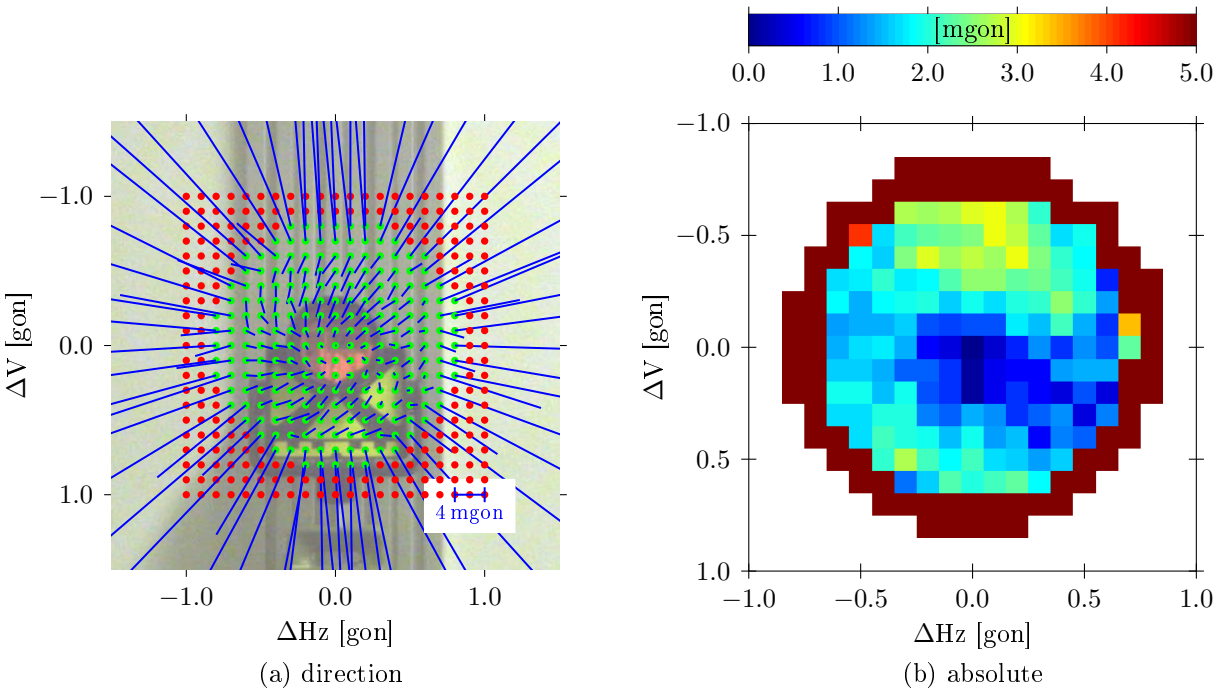

(a) direction (b) absolute

Figure 3-17: ATR errors for a circular prism mounted on T1 ($d = 7.6$ m)

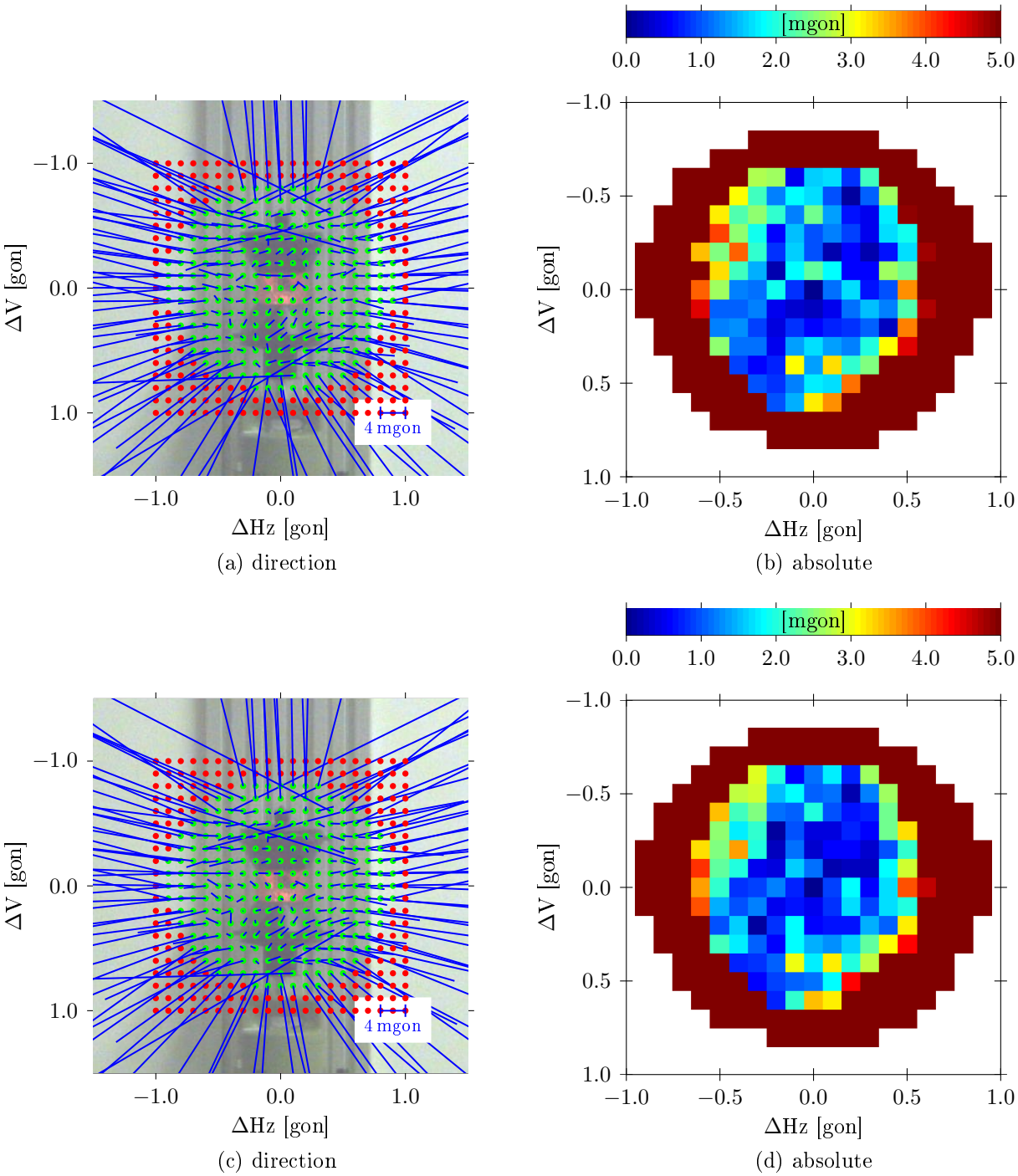

Figure 3-18: ATR errors for a non-rotated 360° prism mounted on T1 ($d = 7.6\,\mathrm{m}$), top line: instrument pointing to a 360° prism, bottom line: instrument pointing to a circular prism

according to the measured ATR corrections. For most accurate measurements, this process is repeated until the ATR corrections are within 5 mgon (cf. section 3.1 for a detailed explanation of the ATR module's operating principle).

Especially the error patterns depicted in figures 3-17 might remind of typical distortion patterns of cameras caused by a radial distortion. Nevertheless, speaking of distortions instead of errors would be misleading since the errors at the boundary area of the field of view are mainly caused by an irregular illumination of the prism (cf. section 3.9.4).

Table 3-3 summarizes the results. The base position accuracies of the ATR module are specified for separations of the optical axis from the prism centre of less than 40 mgon (cf. section 3.2). In the experiments, most of the measurements were made outside this specified area. Due to the large errors at the boundary area of the field of view, the mean and the maximum values of the errors do not fulfil the specifications concerning the base position accuracy. The median of the errors, which is not affected by these large errors, fulfils the specifications perfectly.

At 7.6 m, a measurable angle of 0.6 gon between the main and the auxiliary prism results in a poor maximum separation of roughly 7 cm. However, this distance lies within the range where the wide-angle camera, combined with pattern matching, provides good results (cf. section 5.2). Accordingly, the huge errors at the boundary area do not degrade the accuracy of the system described in this thesis.

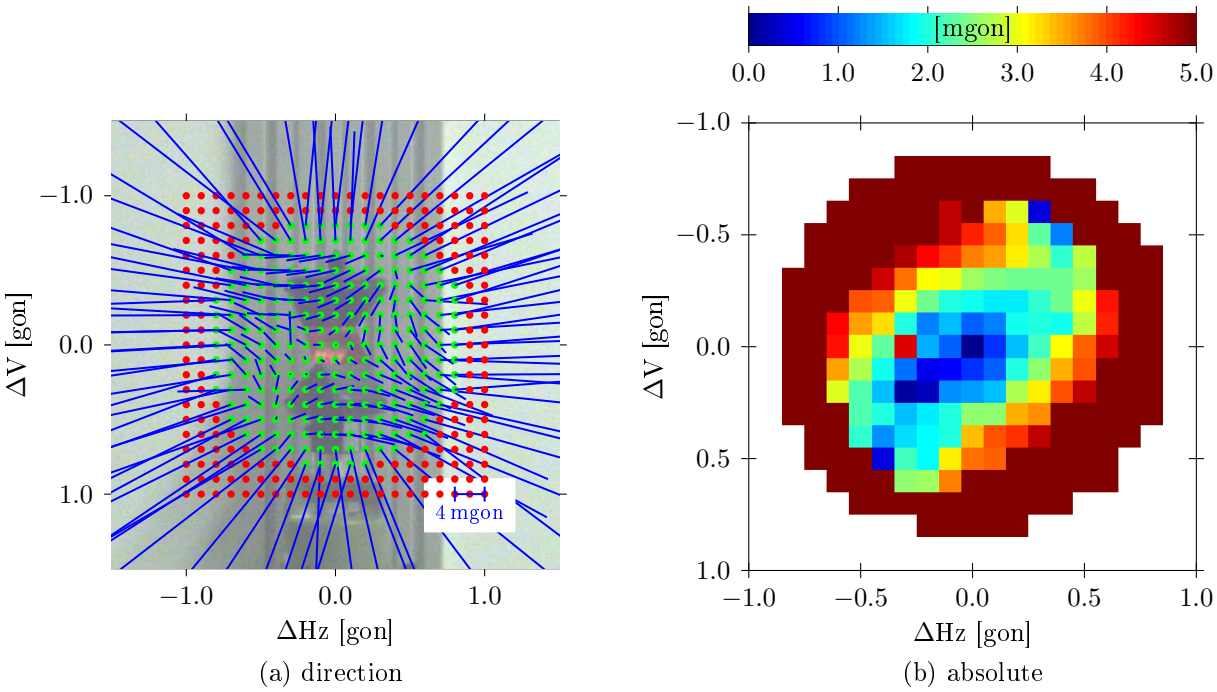

Figure 3-19: ATR errors for a rotated 360° prism mounted on T1 ($d = 7.6$ m)

Table 3-3: Summary of the ATR errors at T1 ($d = 7.6\,\text{m}$) and resulting perpendicular errors (base position accuracies: 1.0 mm circular prism, 2.3 mm 360° prism)

prism	median		mean		max	
	[mgon]	[mm]	[mgon]	[mm]	[mgon]	[mm]
circular	2.1	0.3	15.0	1.8	73.9	8.9
360°	4.8	0.6	32.5	3.9	161.0	19.3
360° set to circular	4.5	0.5	31.9	3.8	160.1	19.1
360° rotated	5.0	0.6	24.0	2.9	111.1	13.3

3.9.2 Medium distances

Contrary to short ($< 25\,\text{m}$) distances, the quality of the ATR measurements in medium distances is relevant to the system described in this thesis because the operating range of the wide-angle camera-based height verification is ending here (cf. section 5.3).

For a circular prism, figure 3-20 shows that, compared to figure 3-17, the errors at the boundary area of the field of view are strongly reduced. The reduction of the errors also applies for a 360° prism. Furthermore, the error patterns of a non-rotated and a rotated 360° prism (cf. figure 3-7) are more similar (compare figure 3-21 to figures 3-18 and 3-19).

For the standard assembling of the modified reflector pole as described in section 1.3, the spot of the auxiliary prism on the ATR module's CMOS array will be located in the area beneath the principal point. Thus, the errors larger than 5 mgon in the corners of the field of view do not degrade the accuracy of the system and the usable field of view may be defined with ± 0.7 gon.

Table 3-4 summarizes the results. At medium distances, the mean value and the median of the errors both fulfil the specifications concerning the base position accuracy of the ATR module. As already depicted in figure 3-21, the negligibility of different rotation states of 360° prism is approved.

At 25.2 m and 40.0 m, a measurable angle of 0.7 gon between the main and the auxiliary prism results in maximum separations of 28 cm and 44 cm, respectively which are both of practical relevance.

Table 3-4: Summary of the ATR errors at T2* ($d = 25.2\,\text{m}$) and T3 ($d = 40.0\,\text{m}$) and resulting perpendicular errors (base position accuracies: 1.0 mm circular prism, 2.3 mm 360° prism)

prism	median		mean		max	
	[mgon]	[mm]	[mgon]	[mm]	[mgon]	[mm]
circular*	1.6	0.6	2.6	1.0	20.6	8.1
circular	0.9	0.5	1.4	0.9	13.4	8.4
360°	1.9	1.2	2.3	1.5	21.2	13.3
360° rotated	1.9	1.2	2.6	1.6	19.1	12.0

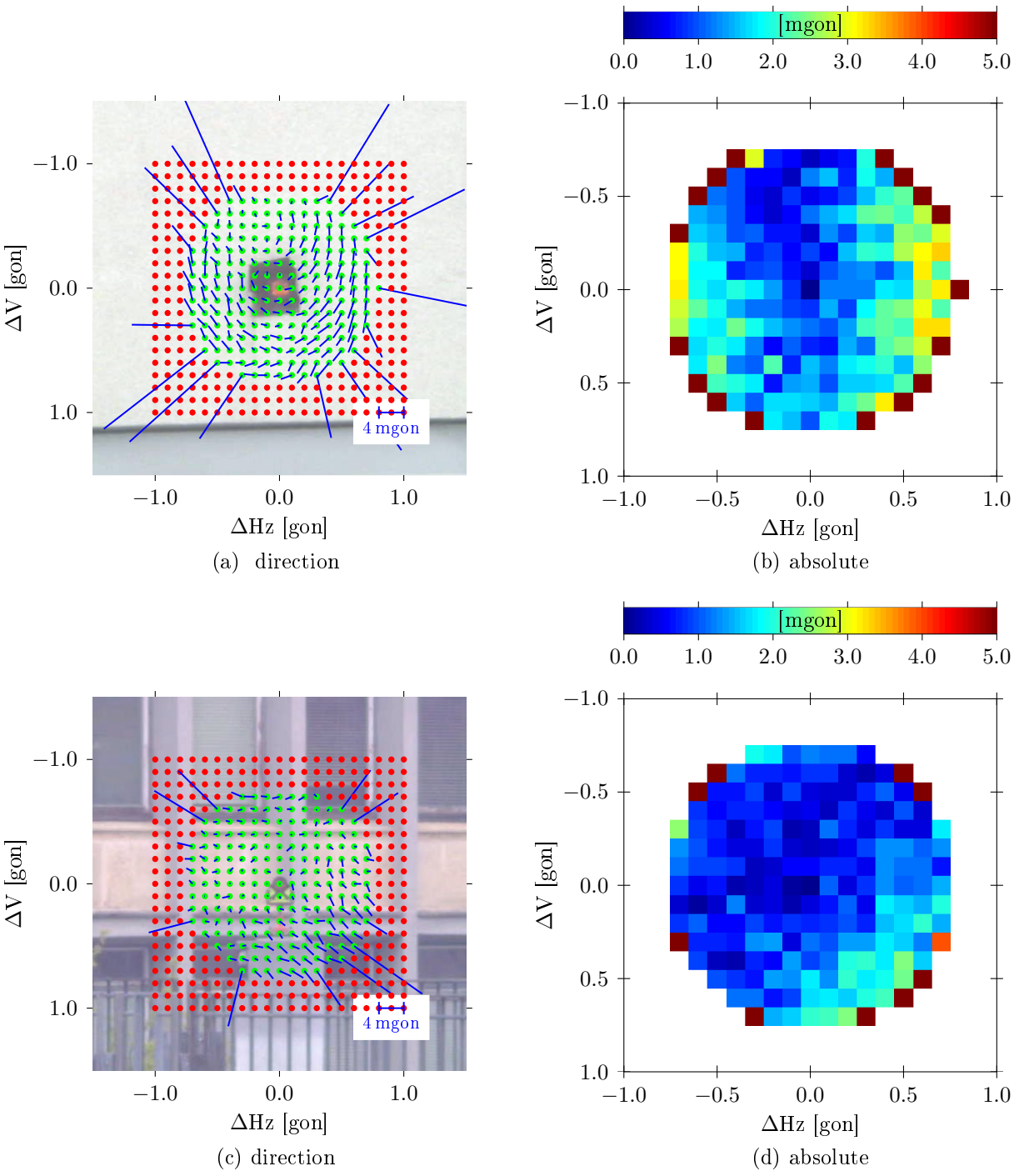

Figure 3-20: ATR errors for a circular prism mounted on T2 ($d = 25.2\,\text{m}$, top line) and T3 ($d = 40.0\,\text{m}$, bottom line)

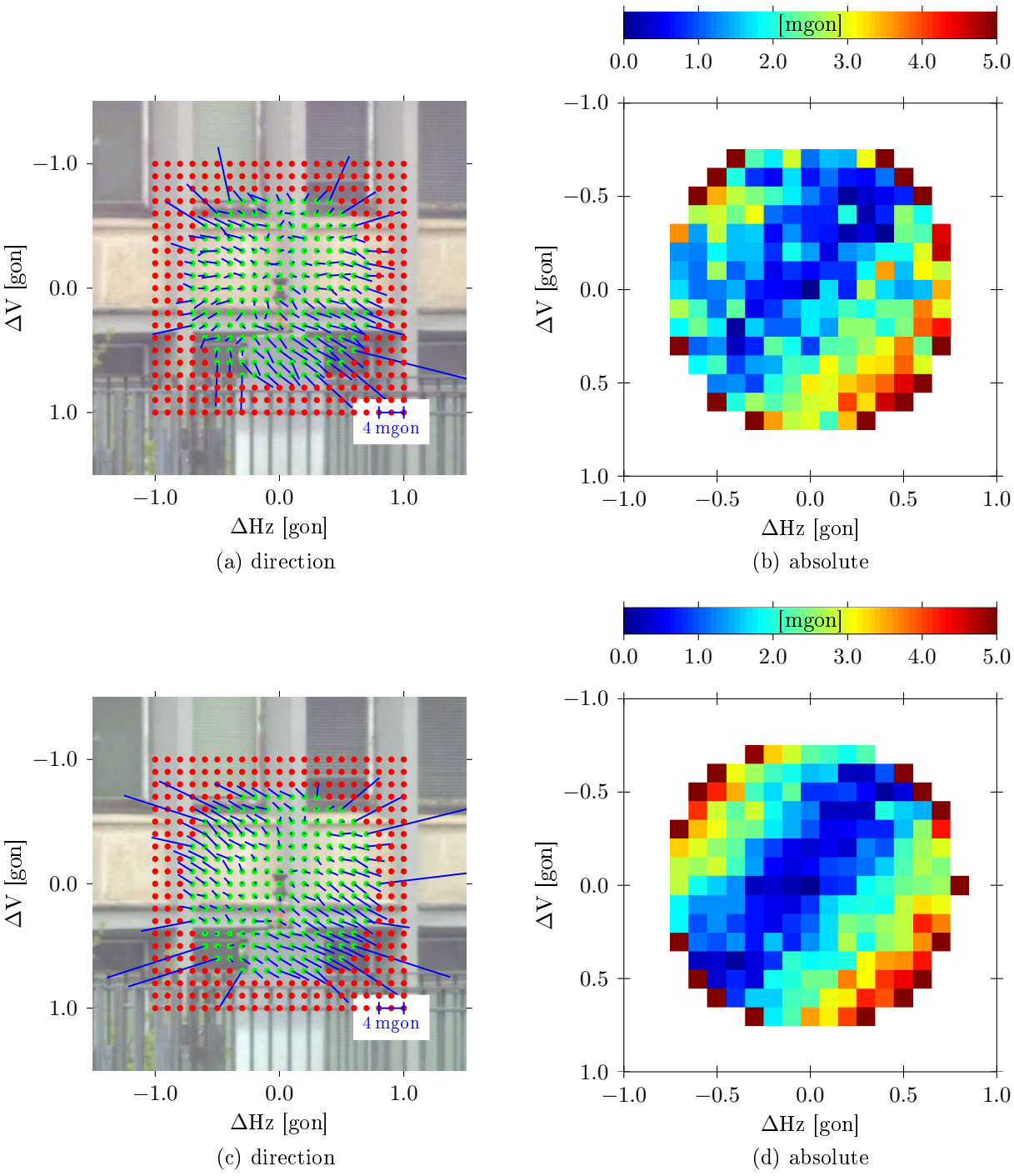

Figure 3-21: ATR errors for a 360° prism mounted on T3 ($d = 40.0\,\mathrm{m}$), top line: non-rotated, bottom line: rotated

3.9.3 Long distances

The quality of the ATR measurements at long distances is of special importance to the operating range of the system described in this thesis since the wide-angle camera-based method does not work here (cf. section 5.3).

For a circular prism, figure 3-22 shows that the errors in the corners of the field of view again decrease (compare with figures 3-17 and 3-20) while the usable field of ±0.7 gon remains unchanged. Contrary to the medium distances (section 3.9.2), the base position accuracy is lower than the computed mean value and median of the errors (cf. table 3-5).

The distance of 215.2 m marks about the range where the accuracy of the angle measurements starts to exceed the base position accuracy (cf. figure 3-3). The ATR accuracy of 1″ is only valid for separations of the optical axis from the prism centre within 5 mgon. For separations up to 40 mgon, the accuracy is specified with 2-3″ (cf. section 3.2 for a detailed discussion of the ATR module's specifications). The separations in this experiment, up to 700 mgon, are far beyond this limiting area.

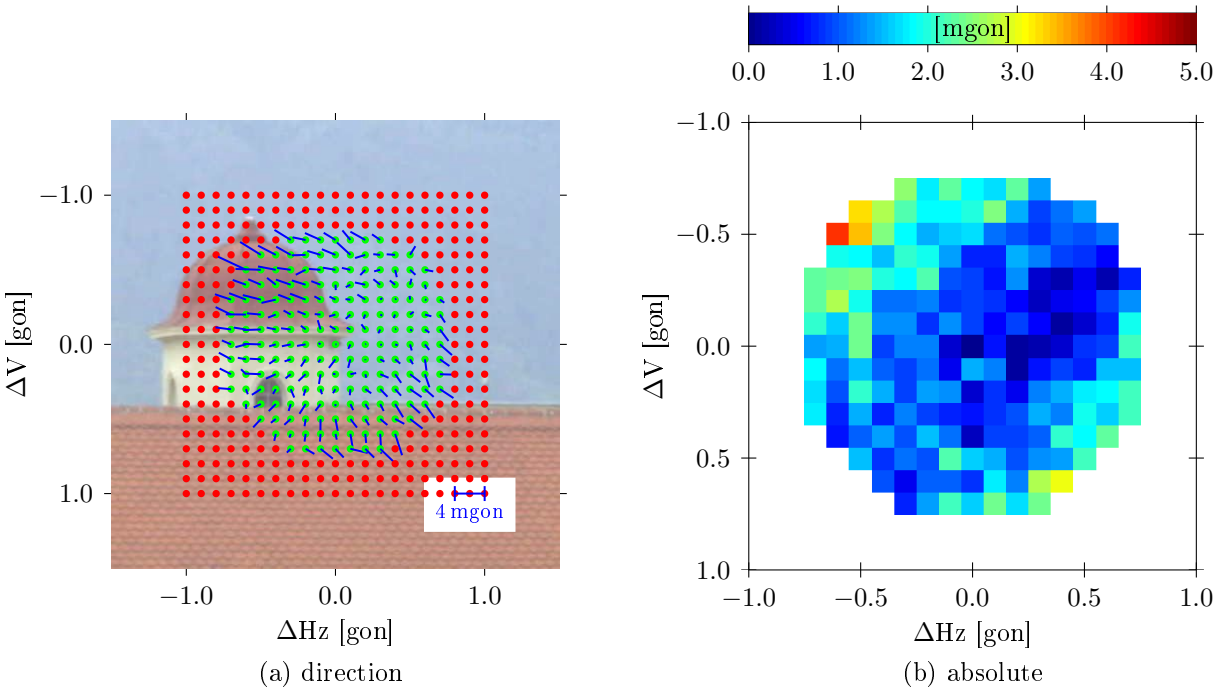

(a) direction (b) absolute

Figure 3-22: ATR errors for a circular prism mounted on T4 ($d = 215.2$ m)

Table 3-5: ATR errors for a circular prism at T4 ($d = 215.2$ m) and resulting perpendicular errors (base position accuracy: 1.0 mm)

median		mean		max	
[mgon]	[mm]	[mgon]	[mm]	[mgon]	[mm]
1.2	4.1	1.3	4.5	4.1	14.0

Nevertheless, the specified value ($3'' \approxeq 0.9\,\text{mgon}$) is close to the computed values of table 3-5. However, errors of less than 5 mm are perfectly sufficient for the aspired accuracy (1 cm, cf. section 1.4) of the system described in this thesis. Errors exceeding 10 mm, possible in the corners of the field of view, are unlikely since the auxiliary prism will never be spotted in these areas when using the standard configuration (cf. section 1.3 for the assembling of the reflector pole).

At distances longer than 100 m, the usable field of view (0.7 mgon) allows separations larger than 1.1 m between the main and the auxiliary prism. For the used prototype, this corresponds to a total reflector pole height of 2.15 m (cf. sections 1.3 and 5.1) which is the maximum height of a standard reflector pole.

3.9.4 ATR errors at the boundary of the field of view

Figure 3-23 shows the increasing errors with increasing separations of the optical axis from the prism centre in greater detail. In contrast to figure 3-16, the visible area of the ATR module is not depicted via an ATR image since, due to the constant focus of the ATR module (cf. section 3.1), it is blurred at a distance of 7.6 m.

In figures 3-23b to 3-23d, the whole prism is imaged on the ATR module's CMOS array but the errors increase with increasing separations. This results from the decreasing illumination of the prism by the emitted IR beam.

For the separation depicted in figure 3-23d, about a fourth of the prism is illuminated by the IR beam. Obviously, the resulting spot on the CMOS array contains not enough information to determine the ATR values via centroid computations and no ATR measurement is possible (cf. section 3.1 for a detailed explanation of the ATR module's operating principle). However, for the separation depicted in figure 3-23c, about the half prism is illuminated by the IR beam and an ATR measurement (yielding bad results) is possible. For the separation depicted in figure 3-23b, the whole prism isn't illuminated neither but the measured ATR values appear to be reasonable.

Analogously to section 3.7, where an external IR source was mounted on the telescope's ocular, figure 3-24 depicts the spots of the prisms on the ATR module's CMOS array for the same separations as in figure 3-23. Although the whole prism is imaged on the CMOS array for all separations, the illumination of the spot becomes more irregular for increasing separations. Compared to figure 3-24a, the intensities of the spot in figure 3-24b are not completely uniform but the deduced ATR values are of good quality (cf. figure 3-23b).

The spots actually processed by the ATR module may differ from the spots depicted in figure 3-24 due to a different IR source. However, it seems that the ATR module does not only use centroid computations to detect the centre of the prism spot on the CMOS array but also utilizes some kind of shape recognition.

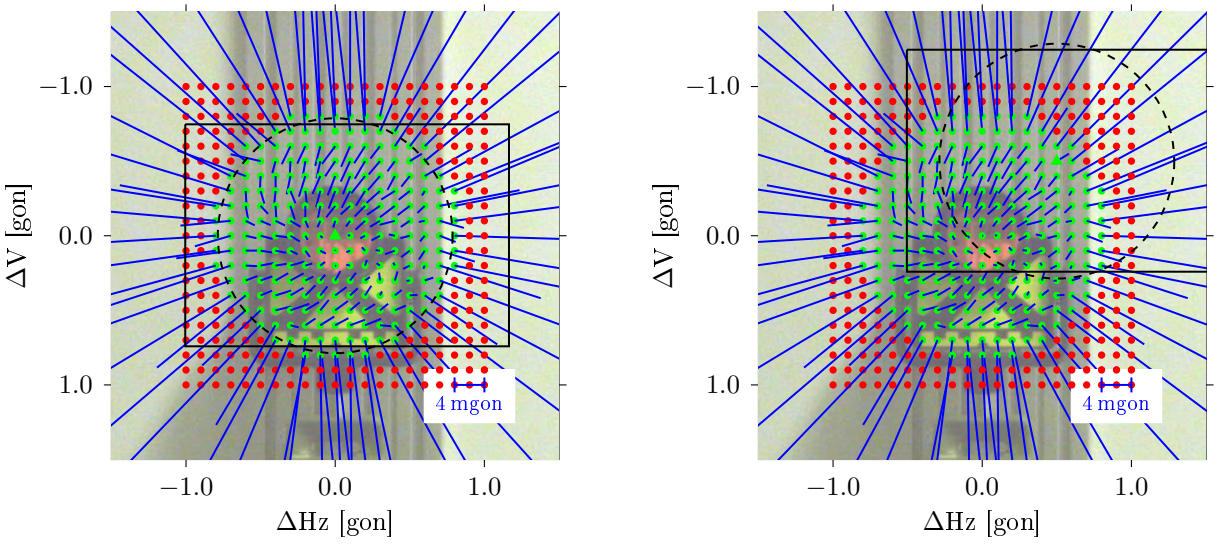

(a) $\Delta\mathrm{Hz} = 0$, $\Delta\mathrm{V} = 0$

(b) $\Delta\mathrm{Hz} = 0.5$, $\Delta\mathrm{V} = -0.5$

(c) $\Delta\mathrm{Hz} = 0.6$, $\Delta\mathrm{V} = -0.5$

(d) $\Delta\mathrm{Hz} = 0.7$, $\Delta\mathrm{V} = -0.5$

Figure 3-23: Visible area of the ATR module's CMOS array (solid, black) and spot of the IR beam (dashed, black) for selected points (triangle), $d = 7.6\,\mathrm{m}$

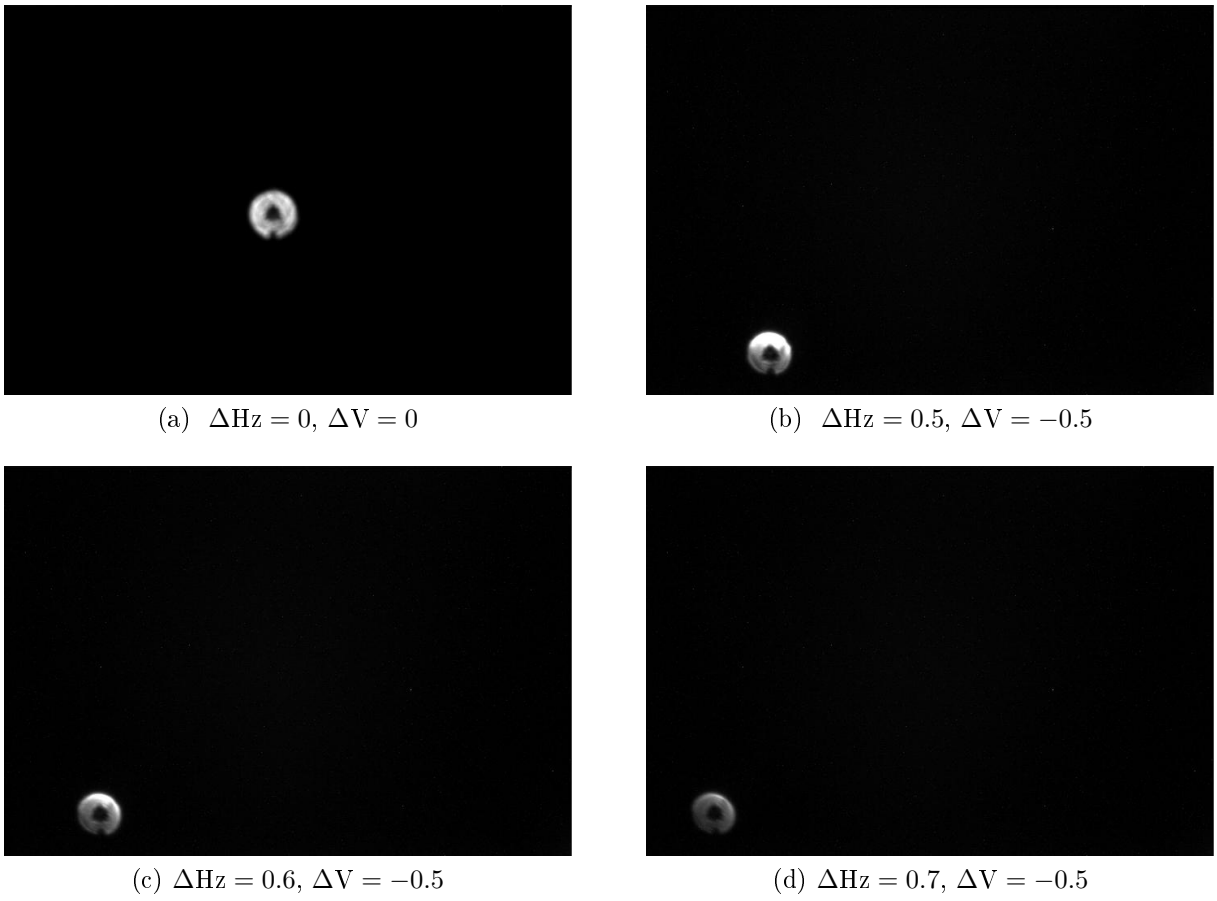

(a) $\Delta\mathrm{Hz} = 0$, $\Delta\mathrm{V} = 0$

(b) $\Delta\mathrm{Hz} = 0.5$, $\Delta\mathrm{V} = -0.5$

(c) $\Delta\mathrm{Hz} = 0.6$, $\Delta\mathrm{V} = -0.5$

(d) $\Delta\mathrm{Hz} = 0.7$, $\Delta\mathrm{V} = -0.5$

Figure 3-24: Prism spots on the ATR module's CMOS array for different separations of the optical axis from the prism centre (illuminated by an externally attached IR source)

3.9.5 ATR errors in the central region of the field of view

The manufacturer specifies the accuracy of the ATR module, dependent on the separation of the optical axis from the prism centre (up to 5 mgon and 40 mgon), with 1″ and 2-3″ (0.6-0.9 mgon), respectively (cf. section 3.2).

The 40 mgon area was investigated using the test routine described in section 3.4. As depicted in figures 3-25a and 3-25b, the specifications are achieved for short and medium distances (except for a few points). For longer distances (figure 3-25c), the specifications could not be verified in this experiment.

Table 3-6 summarizes the results of the experiment. The maximum errors for the short and medium distance are below the base position accuracy of 1 mm (cf. section 3.2). The errors for the long distance exceed this value but the mean error (4.1 mm) is still within the aspired accuracy (10 mm, cf. section 1.4) of the reflector pole height verification. The actual accuracy of the system described in this thesis is investigated in section 5.

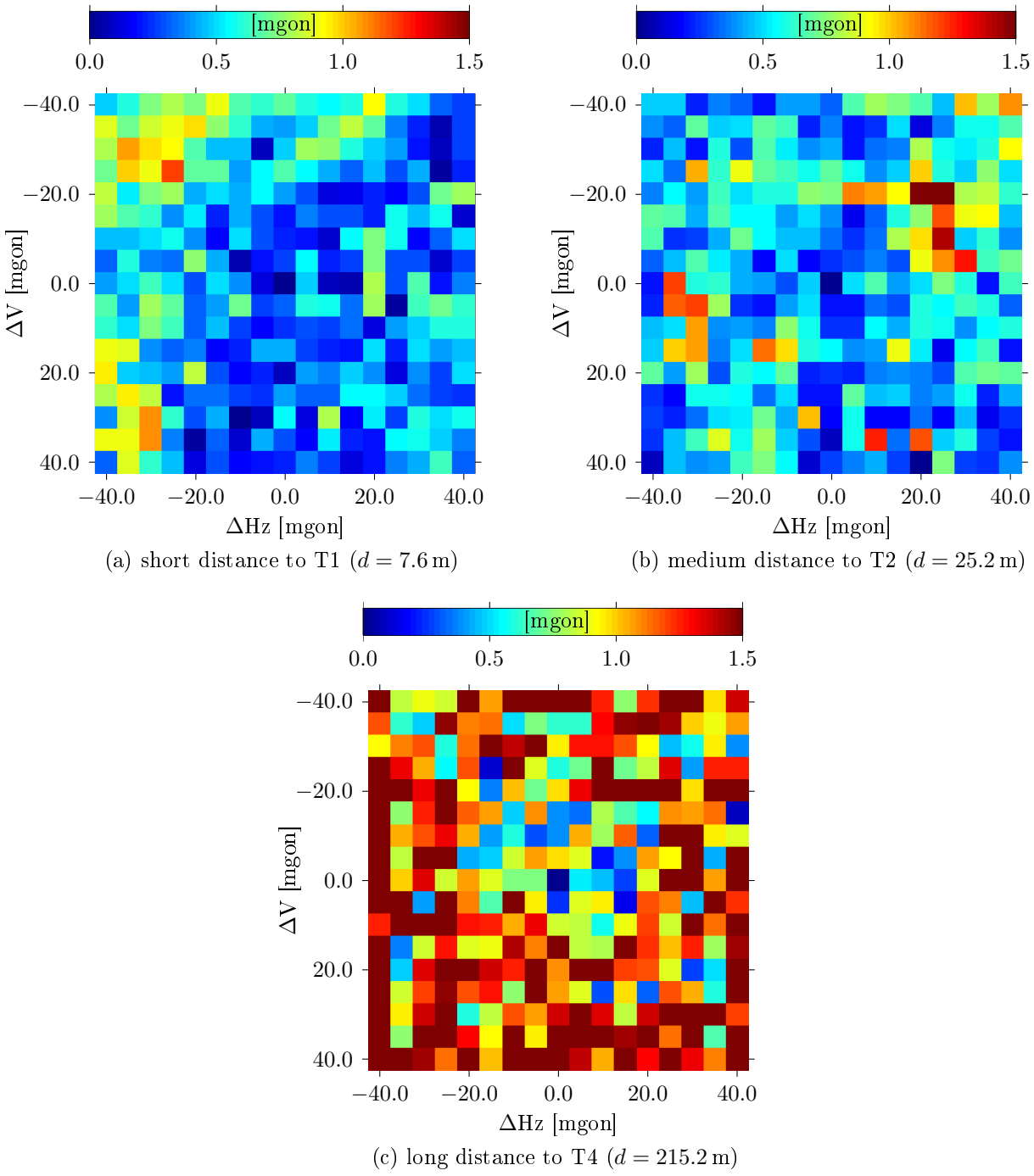

(a) short distance to T1 ($d = 7.6\,\mathrm{m}$)

(b) medium distance to T2 ($d = 25.2\,\mathrm{m}$)

(c) long distance to T4 ($d = 215.2\,\mathrm{m}$)

Figure 3-25: ATR errors for separations of the optical axis from the prism centre up to 40 mgon using a circular prism

Table 3-6: ATR errors for separations up 40 mgon and resulting perpendicular errors

distance	median		mean		max	
[m]	[mgon]	[mm]	[mgon]	[mm]	[mgon]	[mm]
7.6	0.4	0.1	0.5	0.1	1.2	0.1
25.2	0.5	0.2	0.5	0.2	1.5	0.6
215.2	1.2	3.9	1.2	4.1	3.1	10.4

3.9.6 Repeatability of the test measurements

To test the repeatable accuracy of the ATR measurements, two constant configurations were tested at different times of the day. Epoch #1 was measured on 18.04.2012 13:55-14:15 and epoch #2 on 09.05.2012 08:42-09:10.

The differences (#1 - #2) of the ATR errors between the two epochs are given in figure 3-26. Compared to figure 3-20a (epoch #1), the large errors at the boundary area of the field of view vanish in the differences (figure 3-26a) but the clockwise pattern is more intense. This results from the second epoch having counter-clockwise pattern. The differences of the errors depicted in figure 3-26b don't show an obvious pattern.

In figure 3-26a, the reason for the cancelling of the large errors in the corners of the field of view is, that these errors result from an insufficient illumination of the prism (cf. section 3.9.4) which was the same for both epochs.

Since epoch #1 and #2 were measured at different times of the day (noon and morning), the measurements are variably influenced by the sunlight (both epochs were sunny days). However, this should affect the measurements to T4 (figure 3-26b) equally. An ex-

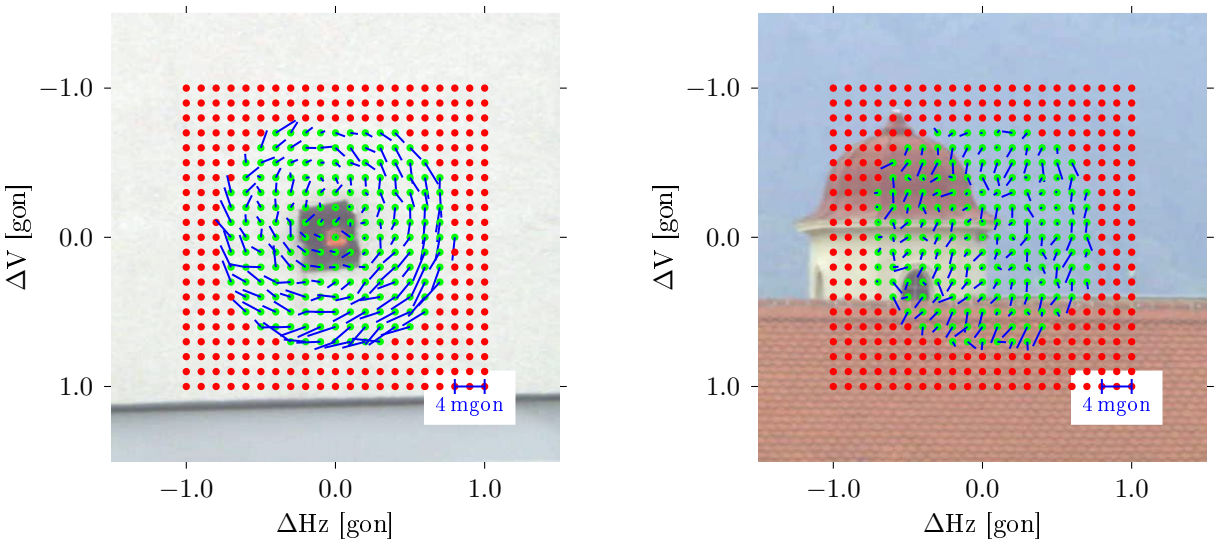

(a) T2 ($d = 25.2\,\text{m}$) (b) T4 ($d = 215.2\,\text{m}$)

Figure 3-26: Differences of the ATR errors between two epochs

planation is found in figure 3-6 which depicts the test area. The sighting to T4 is oriented north-west, i.e. the telescope's objective was shaded from the sun in both epochs (noon and morning). The sighting to T2 is oriented south-east, i.e. the telescope's objective was variably sunlit in both epochs. Since sunlight contains IR light, direct or indirect solar radiation into the telescope's objective can disturb the ATR module's image processing (cf. section 3.1 for the ATR module's operating principle).

Concluding, different light conditions can influence the ATR measurements especially at large separations of the optical axis from the prism centre. Executing ATR measurements in a constant configuration but different light conditions (measurements to T2), resulted in differences of the ATR errors up to 4.5 mgon. For a distance of 25.2 m, this corresponds to a perpendicular of 1.8 mm which is within the aspired accuracy of the reflector pole height verification (10 mm, cf. section 1.4).

3.10 Separability of two prisms

The minimum distance for the verification of the reflector pole height is limited by the ATR module's field of view (cf. section 3.8). According to the manufacturer's specifications (cf. table 3-2), the maximum distance for ATR measurements is limited by the prism type and the measurement mode (single / tracking) where the possible distances vary between 300 m and 1000 m (reflector tape excluded).

However, the maximum distance of the reflector pole height verification may further be decreased by the separability of the spots of the main and the auxiliary prism on the CMOS array (cf. section 1.3 for the assembling of the prototype and section 3.1 for a detailed explanation of the ATR module's operating principle).

To determine the maximum distance between the total station and the targets, at which two prisms, mounted next to each other, may be separated by the ATR module, a

Figure 3-27: Leica GPH3 triple prism holder with two prisms mounted next to each other (73.2 mm separation between the prism centres)

Leica GPH3 triple prism holder was used (figure 3-27). While manually aiming at the left prism (i.e. the main prism in this case), the ATR corrections of the left and right (i.e. the auxiliary prism in this case) prism were recorded. At a certain distance, the ATR module only returned the ATR corrections of one prism, which indicates that the spots of the two prisms could not be separated any more. At this distance, the ATR values of the left prisms were near zero (since the telescope pointed to this prism) which means, that the reflections of the right prism were removed by the ATR module.

Contrary to the assembling of the reflector pole, where the two prisms are separated vertically, they are separated horizontally in this experiment. This should not influence the results since the field of view is given as a diameter (cf. section 3.8) and the ATR errors (in magnitude) rather depend on the absolute separation of the optical axis from the prism centre than on the direction of the separation (cf. sections 3.9.1 to 3.9.3).

Using the slope distance d to the left prism and the horizontal ATR corrections of both prisms $\Delta Hz_{l,r}$, the separation of the two prisms is computed by

$$s_{l,r} = d \tan(\Delta Hz_r - \Delta Hz_l) \tag{3-13}$$

assuming that the triple prism holder is oriented orthogonal to the line of sight and that the two prisms have the same height. For a separation of 73.2 mm between the two prisms (computed by polar measurements to both prisms), an e.g. 10 gon deviation of one of these two assumptions causes an error of 0.9 mm. The differences of the vertical ATR measurements to both prisms are in a range of ± 1 mgon which fulfils the second constraint perfectly. The first constraint, i.e. no rotation around the vertical axis, may not be realized as precisely as the second (with reasonable effort) but 10 mgon, resulting in an acceptable error of less than 1 mm, should be easily possible. However, this issue does not occur in the actual determination of the reflector pole height since the alignment of the two prisms is realized by the circular bubble of the reflector pole.

Figure 3-28 depicts the measured separations of the configuration given by figure 3-27 for different distances. The large deviations from the reference value at a distance of 6 m result from an insufficient visibility of the right prism due to the short distance (cf. section 3.9.4 for more details). The remaining deviations are less than 1 mm which is a remarkable result and gives a first impression of the possible accuracy of the reflector pole height verification. At distances between 110 m and 115 m, the spot of the second prism cannot be separated reliably. A further increase of the distance allows no separation at all. Consequently, the maximum distance of the operating range is limited with 110 m - at least for the minimum possible separation between the two prisms. Section 5.1 investigates the possible operating range for larger separations between the two prisms more extensively.

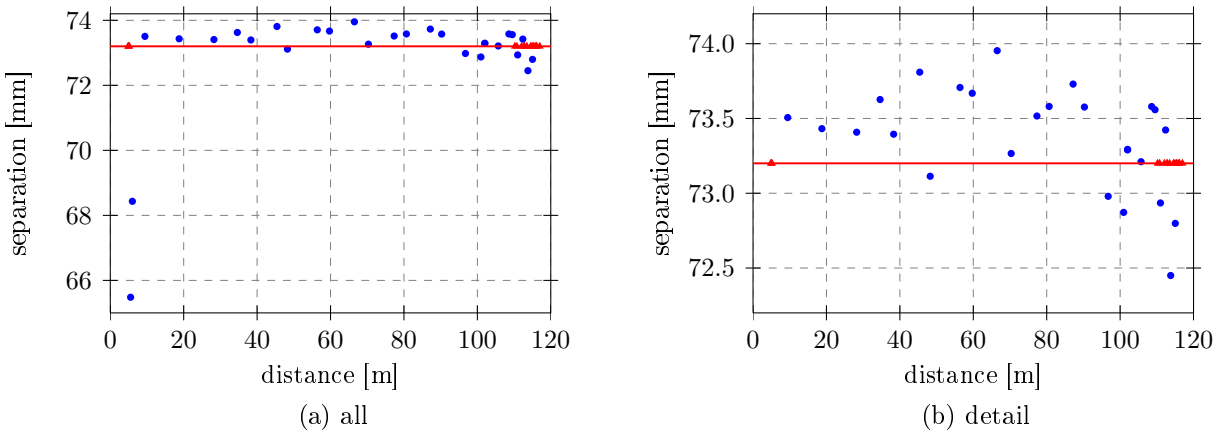

(a) all (b) detail

Figure 3-28: Measured separations (blue) and unsuccessful measurements (red triangle) at different distances compared to the reference value of 73.2 mm (red line)

3.11 Conclusions

For short distances (< 20 m, section 3.9.1), the ATR module can hardly be adopted to determine the reflector pole height since its low aperture angle allows only small (< 0.2 m) separations between the main and the auxiliary prism.

For longer distances (> 25 m, sections 3.9.2 and 3.9.3), the maximum separation between the two prisms (usable field of view) was determined to 0.7 gon yielding average perpendicular errors between 1 mm and 5 mm. In contrast to short distances, undesired effects (e.g. large errors at the boundary area of the field of view, errors due to different orientations of a 360° prism) are reduced to a negligible extent. For the prototype described in section 1.3 and a usable field of view of 0.7 gon, figure 3-29 depicts the operating range of the ATR-based reflector pole height verification. For distances shorter than 25 m, the ATR-based method does not work for any possible reflector pole height (1.3 m to 2.15 m). The maximum reflector pole height of 2.15 m can be measured at a distance of roughly 100 m.

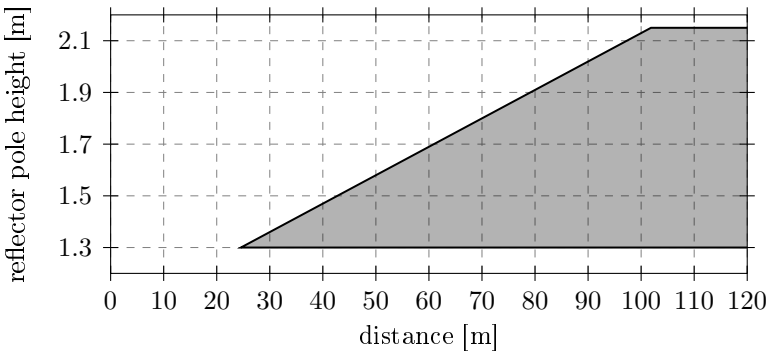

Figure 3-29: Operating range of the ATR-based reflector pole height verification

Improving the system's accuracy by modelling the ATR errors is hardly possible, since they depend on various factors which cannot be captured in practice (e.g. the orientation of a prism cannot be determined at every measured point in a tachymetric surveying). However, errors of the reflector pole height of less than 5 mm for distances between 25 m and 200 m are perfectly sufficient for the aspired accuracy (1 cm, cf. section 1.4) of the system described in this thesis. Table 3-7, which is an extension of table 3-2, summarizes the specification of the ATR module as given by the manufacturer and the results of the experiments described in sections 3.8 to 3.10.

The minimum and the maximum distance, at which the separation between the centres of the main and the auxiliary prism can be measured using the ATR module, depends on the size of the separation. For large separations, the minimum distance increases (which is a drawback), since the auxiliary prism is not within the usable field of view at short distances. The maximum distance increases as well (which is an advantage), since the spots of the two prisms on the CMOS array can be separated at large distances (cf. section 3.10). For small separations, it's the other way round. The operating range for larger separations, which is not given in table 3-7, is investigated in section 5.1.

The differences, concerning the field of view (figure 3-30) and the accuracies, between the manufacturer's specifications and the results of the experiments are not a matter of misinformation but a matter of different usage (discussed in section 3.9.1). The determined accuracies are to be understood as mean values of the ATR errors in the usable field of view (cf. sections 3.9.2 and 3.9.3).

The actual accuracies of the reflector pole heights determined by the system described in this thesis are investigated in section 5. The operating range, using the ATR module and the wide-angle camera, is also investigated there.

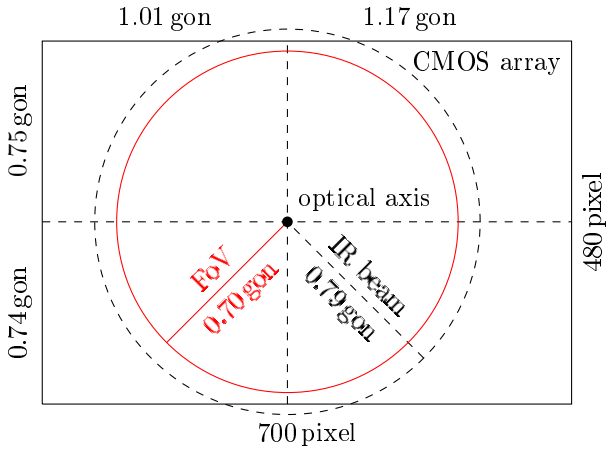

Figure 3-30: Operating range of the ATR module resulting from the CMOS array and the emitted IR beam (black, dashed) compared to the usable field of view (red)

Table 3-7: Extended specifications of the ATR module of the Leica TS15

max. range (ATR/LOCK)[1]	circular prism (GPR1)	1000/800 m
	360° prism (GRZ4, GRZ122)	800/600 m
	mini prism (GMP101)	500/400 m
	360° mini prism (GRZ101)	350/300 m
	reflector tape (60 × 60 mm)	55/- m
	with min. separation (73 mm)	
	of two circular prisms[4]	110 m
min. range[1]	360° prism (ATR/LOCK)	1.5/5 m
	with min. separation (73 mm)	
	of two circular prisms[4]	10 m
max. speed (LOCK)[1]	tangential	5 m/s at 20 m, 25 m/s at 100 m
	radial	5 m/s
prism search[1]	field of view (FoV)	$1°25' = 1.6$ gon
	usable FoV[5]	$1°15' = 1.4$ gon
	typical search time in FoV	1.5 s
accuracy	base position (GPR1/GMP101/ GRZ122/GRZ4)[1]	1/1/2.3/5 mm
	angle within 5 mgon separation[2]	$1''$
	angle within 40 mgon separation[2]	2-3$''$
	angle within 40 mgon separation[6]	2-4$''$
	perpendicular errors within usable FoV[5]	1-5 mm
IR beam[3]	maximum radiant power	10 mW
	pulse duration	11 ms
	pulse repetition frequency	37 Hz
	wavelength	785 nm
	diameter[7]	$1°25'$
light sensitive array[2]	technology	2D complementary metal-oxide-semiconductor (CMOS)
	pixel size	6 μm
	precision of pixel measurement	0.1 pixel
	size (horizontal × vertical)[7]	700 × 480 pixel
	field of view of a single pixel[7]	3.1 mgon/pixel

[1]Leica (2010d, pp. 154-157)

[2]Bayoud (2007)

[3]Leica (2010d, p. 126)

[4]max. and min. distance increase with increasing separation, section 3.10

[5]for distances 25-200 m using a circular prism, sections 3.9.2 and 3.9.3

[6]dependent on the distance, section 3.9.5

[7]section 3.8

4 Investigations on the wide-angle camera

4.1 Specifications of the wide-angle camera

The used total station is equipped with a wide-angle camera (WAC) with the specifications given in table 4-1. Like the ATR module, the wide-angle camera also uses CMOS (complementary metal-oxide-semiconductor) technology. For a short comparison between the CMOS and the CCD technology cf. section 3.1 or see Litwiller (2001) for more detailed informations.

Compared to the usable field of view of the ATR module (1.4 gon diagonal, cf. figure 3-30), the wide-angle camera's vertical field of view (13.0 gon) is much larger. Thus, larger separations between the main prism and the additional target marking (cf. figures 1-1 and 1-2) are possible when using the wide-angle camera. This means a major improvement for the operating range of the system described in this thesis (cf. section 5.3).

The frame rate is important for a smooth display of a moving scene (or when moving the telescope) on the instrument's touch screen. For this purpose, 20 frames per second are absolutely sufficient.

The different zoom levels are not to be understood in the generic sense of standard cameras. If the zoom level is set to e.g. 2x, which is only possible from the total station's user interface (no GeoCOM command), the scene on the instrument's touch screen is reduced to a quarter of the scene at zoom level 1x - so far similar to standard cameras. However, when capturing this image it is stored at zoom level 1x. Thus, the different zoom levels cannot be used for the purposes described in this thesis.

Table 4-1: Specifications of the total station's wide-angle camera (Leica, 2010d, p. 159)

sensor	5 Mpixel 2D complementary metal-oxide-semiconductor (CMOS)
focal length	21 mm
field of view	$15.5 \times 11.7°$ (19.4° diagonal) 17.2×13.0 gon (21.6 gon diagonal)
frame rate	>20 frames per second
zoom	3-step (1x, 2x, 4x)
focus	2 m to infinity at zoom level 1x 7.5 m to infinity at zoom level 4x
image size	640×480 (VGA) 1280×960 (1.2 Mpixel) 2560×1920 (5.0 Mpixel)
field of view of a single pixel[1]	6.8 mgon/pixel (for 5.0 Mpixel)

[1] computed in section 2

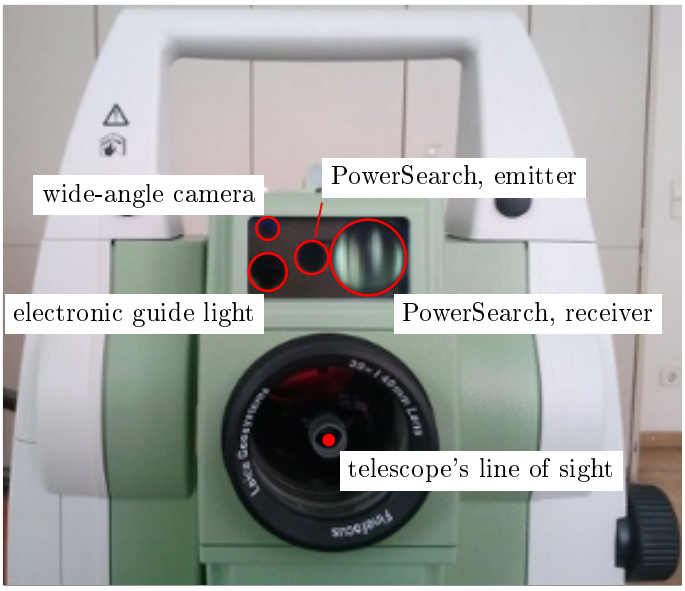

Figure 4-1: Offset between the centres of the telescope and the wide-angle camera

As depicted in figure 4-1, there is an offset between the centre of the telescope and the centre of the wide-angle camera. This offset is determined during the calibration procedure at the production of the instrument and can be read out for the current orientation of the telescope (GeoCOM command `GetCamPos`, cf. Leica, 2010b, p. 96). Furthermore, the optical axes of the telescope and the wide-angle camera are not parallel where the included angle can be computed from the viewing direction of the camera (GeoCOM command `GetCamViewingDir`, cf. Leica, 2010b, p. 97).

4.2 Adopting the wide-angle camera to determine the reflector pole height

The basic idea for adopting the wide-angle camera to determine reflector pole heights is similar to section 3.3. Instead of the auxiliary prism, a fiducial marker is used as a second target marking. Fiducial markers are used in Augmented Reality applications where these markers are observed trough a camera (e.g. a smartphone camera). During the observation, an arbitrary 3D object is virtually placed on the marker and, due to the asymmetry of the marker's coding, may be observed from different positions. For more information on this topic it is referred to Wagner and Schmalstieg (2007) or HandheldAR (2012).

The reason for choosing a fiducial marker as a second target marking is, that open source detection routines for these types of markers already exist. A short introduction to the used software is given in section 4.3.

Furthermore, the knowledge of the marker's size and the image coordinates of its four automatically detected corners are sufficient to compute the orientation and translation

of the marker's coordinate system w.r.t. the coordinate system of the camera (or vice versa). In computer vision, these 6 unknown parameters (3 rotations and 3 translations) are referred to as *pose* (Schweighofer and Pinz, 2005; Kato and Billinghurst, 1999) whereas photgrammetry denotes them as elements of the *exterior orientation* (Kraus, 2004, p. 19). Using the ID of the fiducial marker, up to 4096 different markers (for the BCH encoding) may be identified (for more informations cf. Wagner and Schmalstieg, 2007).

Issues to be clarified are the accuracy and the operating range of the WAC-based height verification (cf. section 5.2).

4.3 Introduction to the marker detection routine

To implement the marker detection routine, two open source libraries were used: OpenCV (v2.4.1) and ARToolKitPlus (v2.1.2). Since both libraries are written in C/C++, they should work on any operating system.

Bradski and Kaehler (2008) and OpenCV (2012a,b) provide detailed informations on OpenCV.

ARToolKitPlus is described in Wagner and Schmalstieg (2007) and HandheldAR (2012). HITLab (2012) provides useful informations on ARToolKit (ARToolKitPlus is the successor of ARToolKit and has many common functionalities).

Figure 4-2 demonstrates the operating principle of the developed marker detection routine (written in C++).

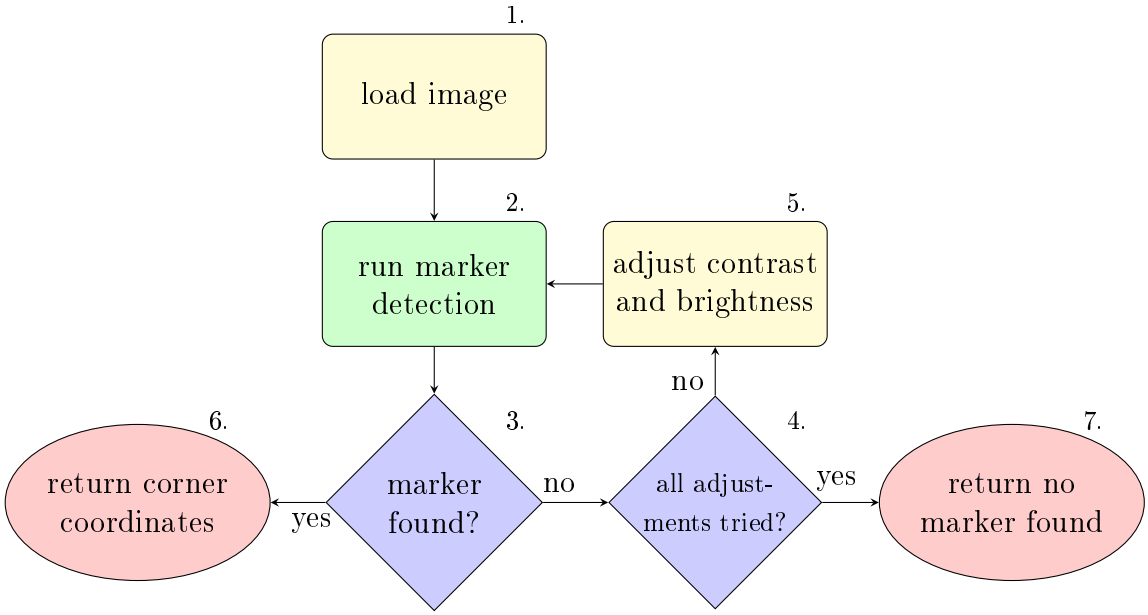

Figure 4-2: Simplified flowchart of the marker detection routine with OpenCV (yellow) and ARToolKitPlus (green) operations

1. The image captured by the total station's camera is loaded using OpenCV functionality.

2. Using ARToolKitPlus, markers are searched where the threshold for converting the original image to a binary image (black and white) is automatically set. If no marker is found in the first place, the threshold is randomized (Wagner and Schmalstieg, 2007). This randomization is repeated 10 (empiric number) times.

3. All detected markers are checked whether their horizontal coordinate corresponds to the horizontal image centre with a tolerance of ±5% (empiric number) of the image width. If a marker fulfils this criterion, it lies roughly within the same vertical as the main prism and thus is very likely to be the true marker (6.). Since there is still the possibility of having a wrong marker detected in this way, plausibility checks on the resulting reflector pole height should be performed.

4. If no marker according to the criterion of 3. is found, a set of empiric values for contrast and brightness is used to manipulate the original image (5.). If all attempts fail, no marker detection is possible (7.).

5. Using OpenCV functionality, the contrast and brightness of the original image is changed before another marker detection.

6. The marker's image coordinates are passed to MATLAB for further processing.

7. The marker detection failed and no computation of the reflector pole height is possible.

To optimize ARToolKitPlus for the purposes of this thesis, slight modifications in its source code were made (cf. appendix A). The OpenCV libraries remained unchanged.

4.4 Conclusions

From the wide-angle camera's half field of view (6.5 gon, cf. table 4-1) and the size of the fiducial marker (8×8 cm, the whole marker must be visible in the image for a successful detection), the minimum operating range of the WAC-based reflector pole height verification can be deduced. For the prototype described in section 1.3, this is depicted in figure 4-3 where the offset between the centre of the telescope and the centre of the camera and the skewness of the two optical axes (telescope and camera) are not considered (cf. section 4.1). The minimum operating range of the system described in this thesis is improved by using the wide-angle camera for the reflector pole height verification (compare figures 3-29 and 4-3).

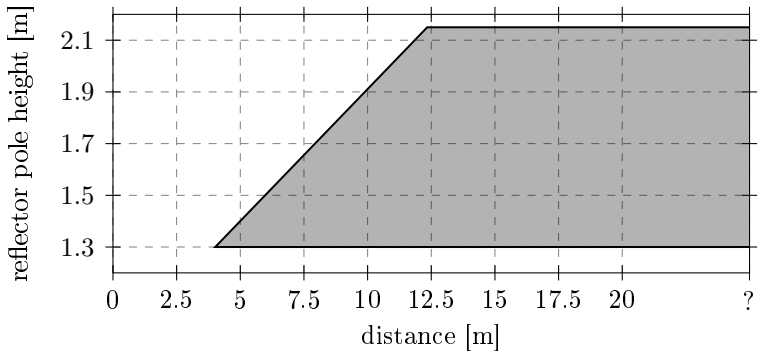

Figure 4-3: Approximate operating range of the WAC-based reflector pole height verification

The maximum operating range and the achievable accuracy of the WAC-based reflector pole height verification need to be determined. These two issues are clarified in section 5.2. The possible operating range of the system described in this thesis, resulting from a combination of the ATR module and the wide-angle camera, is given in section 5.3.

5 Test measurements

To determine the accuracy and the operating range of the system described in this thesis, test measurements were carried out. The measurements took place between 30.07.2012 and 03.08.2012 at different times of the day (09:30-19:30). The test tracks are depicted in figure 5-1.

5.1 ATR-based

From section 3, accuracies of a few millimetres are to be expected from the ATR-based height determination - at least for distances shorter than 200 m. Issues to be clarified are the maximum distance with a reflector pole height of 1.3 m (minimum height) due to an overlapping of the two prism spots (cf. section 3.10) and the minimum distance with a reflector pole height of 2.15 m (maximum height) due to the usable field of view of the ATR module (cf. section 3.11).

The determined reflector pole heights were compared to their "true" value gained from polar measurements to the main and the auxiliary prism. Due to provisional assembling of the used prototype (cf. figure 1-2), the separation between the two prisms changed during long transportations. Thus, the reference heights were measured before and after each test measurement where differences of less than 0.3 mm occurred.

The errors (measured height - reference height) resulting from the test measurements with a reflector pole height of 1.3 m are depicted in figure 5-2. Using the prototype described in section 1.3, a total height of 1.3 m corresponds to roughly 0.27 m separation between the main and the auxiliary prism.

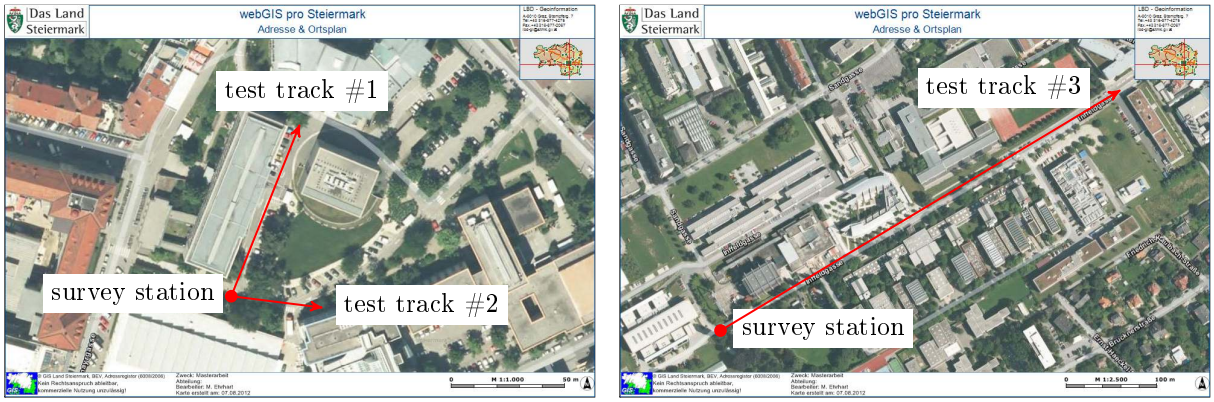

(a) Campus Neue Technik (b) Inffeldgasse

Figure 5-1: Sightings for testing the reflector pole height determination (orthophoto source: www.gis.steiermark.at)

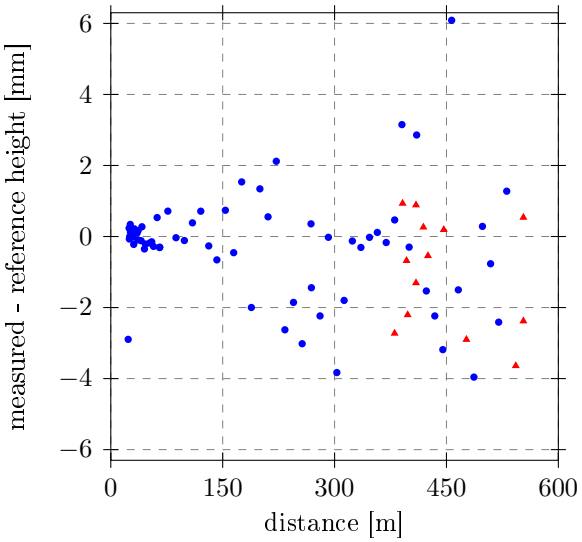

Figure 5-2: Errors for a reflector pole height of 1.3 m

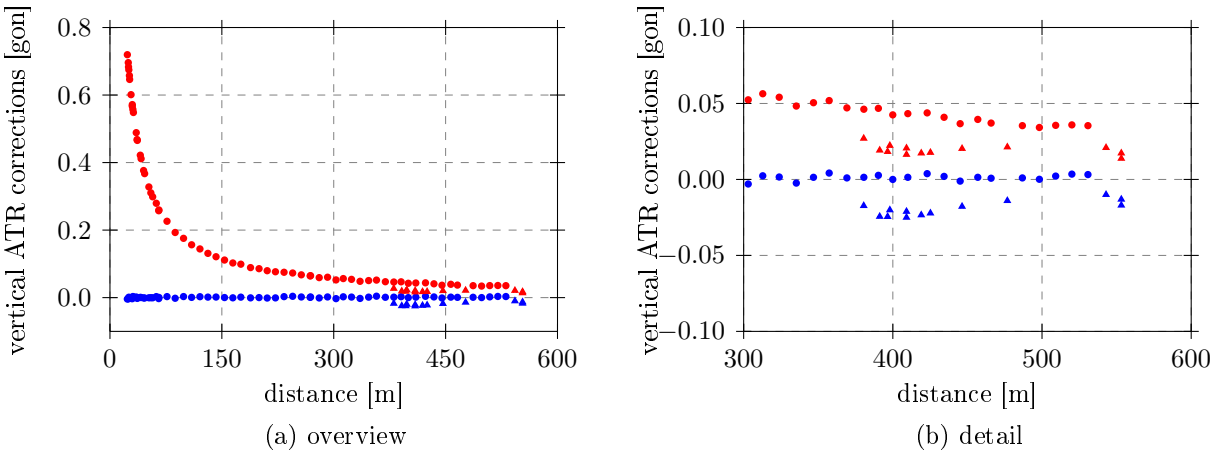

Figure 5-3: Vertical ATR corrections of the main (blue) and the auxiliary (red) prism

During the test measurements, it could be observed that the ATR module, for distances longer than 380 m, sometimes did not aim at the centre of the main prism but on the centroid of the main and the auxiliary prism. Distance measurements were possible nevertheless. In fact, for measuring long (>1 km) distances, more than one prism is used (e.g. with a triple prism holder, cf. figure 3-27) since more of the emitted signal is backscattered by three prisms than by one.

The cases where the telescope is positioned at the centroid may be identified by investigating the vertical ATR values (figure 5-3). When aiming at the centre of the main prism, the vertical ATR correction of the main prism is close to zero where the correction of the auxiliary prism is separated. When aiming at the centroid of the main and the auxiliary prism, these corrections are both separated by roughly the same value (in opposite directions). This provides a possibility to identify such cases. In figures 5-2 and 5-3,

these measurements are accented by a red triangle while the measurements in standard configuration (aimed at the main prism) are accented by a blue dot.

By using the vertical ATR corrections of the main and the auxiliary prism for the determination of the reflector pole height (cf. figure 2-2), aiming not precisely at the centre of the main prism does not influence the results. However, the actual height of the measured point will be affected if the measured zenith angle is not corrected by the ATR correction of the main prism.

In figure 5-2, the eye-catching height error at a distance of 23 m is explained by an insufficient illumination of the prism by the ATR module (cf. section 3.9.4). The height error at a distance of 457 m is an outlier according to the 3s-method. Both errors are not considered in further computations.

Figure 5-2 depicts furthermore, that the magnitude of the errors is roughly constant for distances shorter than 170 m. Afterwards, the magnitude starts to increase. At a distance of roughly 200 m, the accuracy of the angular measurement starts to take over the base position accuracy of the ATR module (cf. figure 3-3). This is again depicted in figure 5-4 where the accuracy given by the manufacturer (1 mm base position and 1″ afterwards) is multiplied by $\sqrt{2}$ to account for the fact that two ATR measurements are used to determine one height. Note that the two outliers from figure 5-2 are removed and no distinction is made whether the telescope was aimed at the centre of the main prism or at the centroid of the main and the auxiliary prism.

Some errors slightly exceed the theoretic accuracy. As described in section 3.2, an accuracy of 1″ is only valid if the separation of the telescope's optical axis from the prism centre is less than 5 mgon. The measured separations are far beyond this limiting value (cf. figure 5-3a). Since the errors' magnitude alternates with the distance between the total station and the targets, the accuracies of the system described in this thesis are also related to the distance (table 5-1).

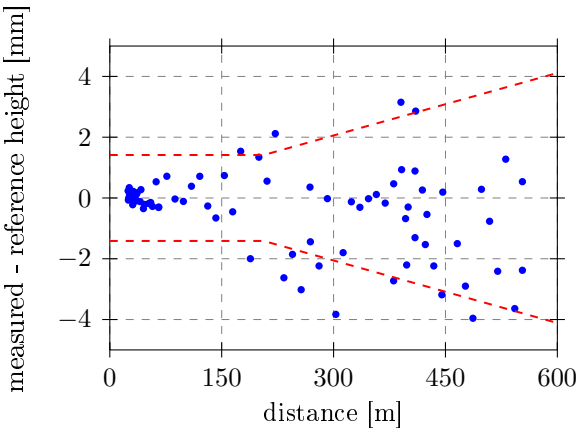

Figure 5-4: Errors for a reflector pole height of 1.3 m and theoretic ATR accuracy ($\cdot\sqrt{2}$)

Table 5-1: Standard deviations of the reflector pole height verification (1σ)

25 to 200 m:	0.6 mm
200 to 550 m:	1.8 mm
25 to 550 m:	1.4 mm

The range, at which no height measurements are possible any more, could not be determined due to a lack of a long enough test track within a economically reachable distance. In section 3.10, two prisms (separated by 0.073 m) could be detected for distances up to 110 m which corresponds to an angle of roughly 0.04 gon. For the separation used in the test measurements (0.27 m) and a distance of 550 m, the angle between the two prisms is roughly 0.03 gon where the 0.04 gon of section 3.10 only correspond to a maximum distance of 430 m. Consequently, the relation between the separation of the main and the auxiliary prism and the distance is non-linear. Although the possible operating range of the ATR module (up to 1 km, cf. table 3-2) may presumably not be fully reached, a maximum distance of longer than 550 m may be expected. However, the tested 550 m should be sufficient for most practical purposes.

For a reflector pole height of 2.15 m (maximum height of a standard Leica reflector pole), the separation between the main and the auxiliary prism of the prototype corresponds to 1.12 m (cf. section 1.3). For the maximum reflector pole height, the main issue was to determine the minimum distance between the total station and the targets for measurements to be possible. Gaining bad results (error of a few millimetres due to an insufficient illumination of the auxiliary prism, cf. section 3.9.4), a measurement was possible for a distance of 97 m. At 99 m, the error was less than one millimetre. Knowing from the test measurements with a reflector pole height of 1.3 m, that the errors primarily depend on the distance, the accuracies of table 5-1 should also hold true for a reflector pole height of 2.15 m. The operating range is limited to distances longer than 100 m. It should be kept in mind, that the system described in this thesis does not account for any inclination of the reflector pole. Thus, an inclination affects large reflector pole heights more than smaller ones.

The test measurements verify the conclusions made in section 3.11 where the maximum separation between the main and the auxiliary prism, at which ATR measurements are possible within reasonable accuracy, was determined to 0.7 gon. This value corresponds to 0.27 m and 1.12 m (tested separations between the main and the auxiliary prism) at distances of 24.6 m and 101.9 m, which are roughly the minimum distances determined in the test measurements (25 m and 99 m).

5.2 WAC-based

Contrary to the ATR-based method of the reflector pole height verification, no preliminary experiments, which allow an estimation of the possible accuracy or the operating range, were made for the WAC-based method. Similar to the ATR-based method, test measurements with the minimum (1.3 m) and the maximum height (2.15 m) of a standard Leica reflector pole were carried out. For the prototype described in section 1.3, these heights correspond to 0.37 m and 1.22 m separation between the main prism and the centre of the fiducial marker (size: 8×8 cm, border width: 1 cm), respectively. Again, these reference heights were determined by polar measurements to the main prism and the fiducial marker before and after each test where differences less than 0.6 mm occurred.

To start with some of the results, measurements were possible up to roughly 25 m. For some images, this could only be achieved by changing the brightness if no marker was detected in the original image. Using the standard settings of the marker detection routine, an inhomogeneous illumination of the fiducial marker (cf. figure 5-5) causes the detection to fail - especially at short distances. Therefore, the threshold, which is used to convert the original image to a binary image (black and white), was chosen to be automatically set and altered if necessary. An alteration of the threshold is only made if no marker is found in the first place. For the used test area (cf. figure 5-1), especially windows of buildings were very likely to be detected as (false) markers. Thus, a sharper criterion for the detection of a valid marker was set. The functioning of the marker detection routine is described in section 4.3 and a summary of the modifications in the used libraries is given in appendix A.

Figure 5-5: Auxiliary prism partly shadowing the fiducial marker at a distance of 4.6 m

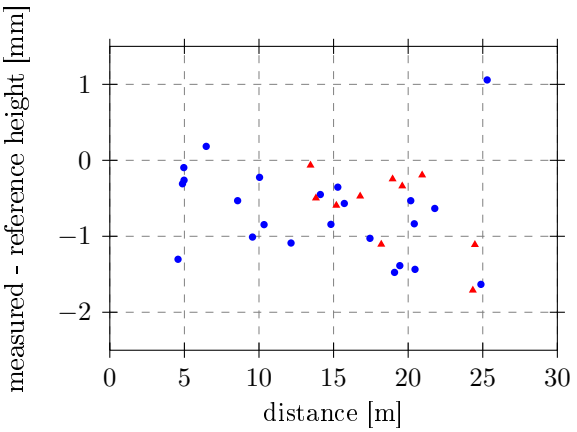

Figure 5-6: Errors for reflector pole heights of 1.3 m (blue dot) and 2.15 m (red triangle)

Figure 5-6 depicts the temporary results for the WAC-based height verification. The slight trend indicates errors in the used model (taken from eq. 2-2)

$$\alpha = \omega \, (y_{\text{marker}} - y_{\text{prism}}) \tag{5-1}$$

for computing the angle between the main prism and the marker. Remembering that the total station's wide-angle camera is primarily designed for documentation purposes, some components may not be assembled or calibrated as precisely as components used for measurements. The slope of the linear trend in figure 5-6 indicates an error in the angle between the telescope's and the camera's optical axes. Thus, eq. 5-1 is extended to

$$\begin{aligned} \alpha &= \omega \, y_{\text{marker}} - (\omega \, y_{\text{prism}} - \gamma) \\ &= \omega \, (y_{\text{marker}} - y_{\text{prism}}) + \gamma \end{aligned} \tag{5-2}$$

where γ denotes the error in the (vertical) angle between the telescope's and the camera's optical axes which influences the pixel coordinates of the main prism (cf. section 2 for details on the operating principle of the height determination).

Regarding eq. 5-2 and the formula for the height determination (taken from eq. 2-4)

$$h = d^* \frac{\sin \alpha}{\sin \beta} + \epsilon \, \cot \beta \tag{5-3}$$

where $\beta = V + \alpha + \delta$, the derivative w.r.t. γ reads

$$\partial h / \partial \gamma = d^* \left(\frac{\cos \alpha}{\sin \beta} - \frac{\sin \alpha \, \cos \beta}{\sin^2 \beta} \right) - \frac{\epsilon}{\sin^2 \beta}. \tag{5-4}$$

A parameter adjustment of γ was done using the data of figure 5-6 where the outlier at a distance of 25 m (according to the 3s-method) was not considered. This resulted in

$\gamma = 2.9 \pm 0.3$ mgon (1σ). Using eq. 5-2 and the adjusted value for γ, figure 5-7 depicts the final results for the determined heights based on wide-angle camera measurements (the outlier at 25 m is not depicted).

The standard deviation of the errors is 0.4 mm for the entire operating range (no alternation as in ATR-based method, cf. figure 5-4 and table 5-1) which is limited to a maximum distance of 25 m (for any possible reflector pole height). The minimum distances are 4.5 m and 13.5 m for reflector pole heights of 1.3 m and 2.15 m, respectively.

Figure 5-8 depicts the vertical image coordinates of the detected markers corresponding to the errors of figure 5-7. The image coordinates of the markers resulting from measurements at the shortest distances of the operating range are in the lower boundary area of the image (image resolution 2560×1920 pixel). At the boundary area of images, distortions (primarily the radial distortion, cf. Kraus, 2004, p. 52) of cameras have the largest effect. However, the errors of the reflector pole heights resulting from markers captured at the boundary area of the image are similar to the errors resulting from markers captured at

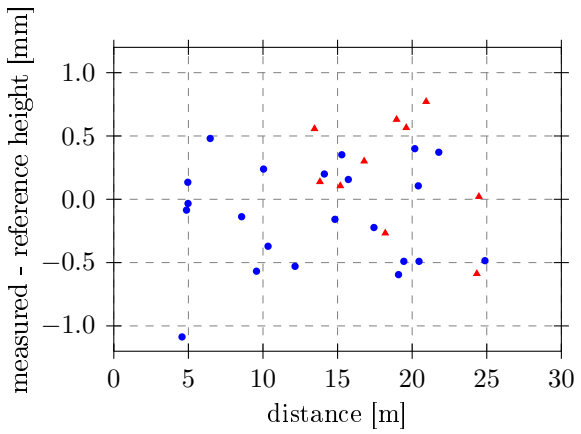

Figure 5-7: Errors for reflector pole heights of 1.3 m (blue dot) and 2.15 m (red triangle) with estimated γ

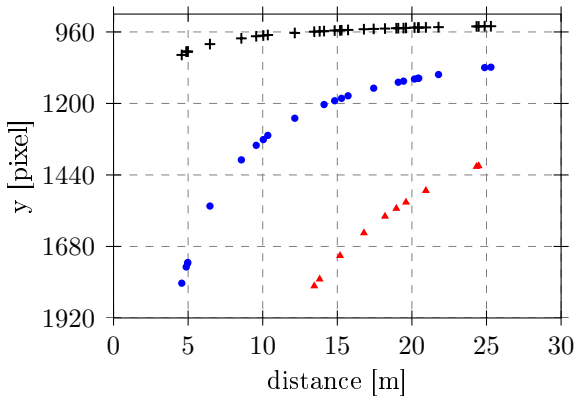

Figure 5-8: Vertical image coordinates of the optical axis (black cross) and the centres of the detected markers for reflector pole heights of 1.3 m (blue dot) and 2.15 m (red triangle)

more central regions (compare figures 5-7 and 5-8). Thus, a calibration of the wide-angle camera is not necessary for the purpose described in this thesis.

Concluding, the minimum distance for height measurements using the WAC-based method is limited by the criterion of the whole marker being visible to the wide-angle camera. This may be computed from the camera's (vertical) field of view and the marker size. The maximum distance (25 m in the test measurements) could presumably be enhanced by spending more time on image manipulation (e.g. further changes of contrast and brightness or appliance of different filters). However, this would also slow down the process of the marker detection. Except for using a larger fiducial marker or a camera with a higher resolution, another possibility for extending the maximum distance could be the usage of a different type of marker. Figure 5-9 shows the appearance of the marker in wide-angle camera images for selected distances. Using a marker with a thin (1 cm) border causes the white parts of the marker to disturb its border at long (> 25 m) distances (top right corner in figure 5-9c). This can be avoided by using a thicker border or even a black square on a white background. Using a black square, the ability of identifying different markers using their ID is lost (cf. section 4.2). Furthermore, the white background needs a sufficient width to avoid a disturbance caused by pixel of the surrounding area.

In fact, using a marker of the same size as in the test measurements (8×8 cm) but with a 2 cm border (instead of 1 cm), the detection worked for distances up to 40 m (indoors). However, this thesis is meant as preliminary work for the possible development of a market-ready system. For practical purposes, the additional targets on the reflector pole should be as small as possible which was the reason for choosing a thin border rather than a thicker one (cf. figure 7-1 for a design study of a market-ready reflector pole).

(a) 5.0 m: detection worked (b) 24.9 m: detection worked (c) 26.4 m: detection failed

Figure 5-9: Appearance of the fiducial marker (not to scale) in wide-angle camera images for different distances

5.3 Critical configurations

Concerning accuracies and using the model of eq. 5-2, the WAC-based method for the reflector pole height verification can almost compete with the ATR-based method. For a reflector pole height of 1.3 m, this is depicted in figure 5-10 where the values for the ATR-based method stem from figure 5-4 and those for the WAC-based method from figure 5-7.

Figure 5-11 depicts the operating range of the prototype described in section 1.3. For a reflector pole height of 1.3 m, the systems works for distances larger than 4.5 m without interruptions (this is also depicted in figure 5-10). Using a reflector pole height of 2.15 m strongly limits the operating range where the accuracies remain unchanged (cf. sections 5.1 and 5.2). The range from roughly 25 m to 100 m in figure 5-11, where no height verification is possible for a reflector pole height of 2.15 m, results from the small usable field of view of the ATR module (half FoV: 0.7 gon, cf. section 3.11) and the low maximum distance of the WAC-based height verification (25 m, cf. section 5.2).

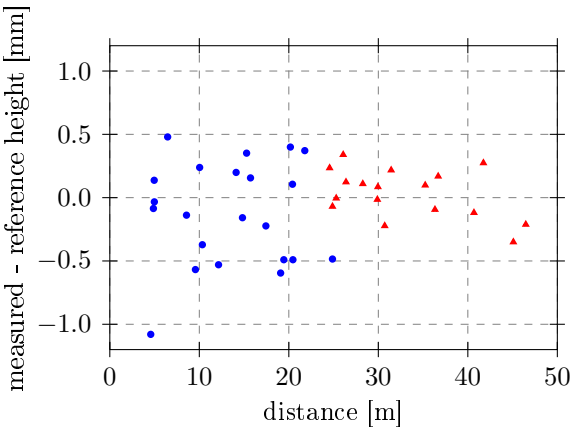

Figure 5-10: Height errors for a reflector pole height of 1.3 m using the WAC-based (blue dot) and the ATR-based (red triangle) method

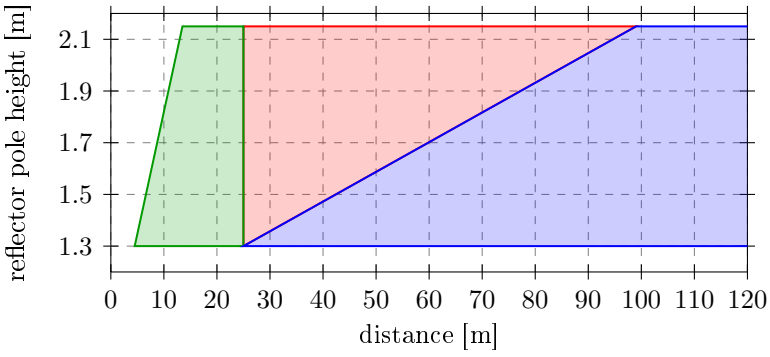

Figure 5-11: Operating range of the prototype using the WAC-based (green) and the ATR-based (blue) method and critical configurations (red)

With height errors of less than 5 mm for distances up to 550 m (cf. section 5.1), the accuracy and the maximum range are already sufficient for practical purposes (discussed in section 1.4). Aiming at market-ready, thoroughly working system, i.e. no interruptions of the operating range after a certain (as short as possible) distance, these gaps need to be eliminated for all possible reflector pole heights. Some approaches are discussed in section 7.

If neither the ATR-based nor the WAC-based height verification works, there is still the possibility of a second polar measurement to the auxiliary prism. This would provide the most accurate results but is too slow and impractical (since the telescope needs to be moved whilst the pole must not move) to be implemented as the standard measuring mode.

6 Conclusions

In this thesis, the prototype of a system for the automatic detection of wrong reflector pole heights has been described. The system leaves the measurements exclusively to the total station (Leica TS15, cf. section 1.5), i.e. no electronic devices for measuring the height and transferring it to the total station are required at the reflector pole. Instead, the system uses the total station's ATR module (cf. sections 3 and 5.1) and its built-in wide-angle camera (cf. sections 4 and 5.2). The system was tested to a maximum distance of 550 m where errors of less than 5 mm in the measured reflector pole heights occurred. The maximum distance, which may presumably be extended (cf. section 5.1), and the accuracy are believed to fulfil the requirements of most practical purposes (cf. section 1.4).

For a reflector pole height of 1.3 m, the system works for distances longer than 4.5 m without interruptions - provided that the sighting from the total station to the used components is not obstructed (cf. section 1.4). Extending the reflector pole to the maximum height of 2.15 m causes a gap in the operating range from 25 m to 100 m (cf. section 5.3). However, it is believed that this gap may be eliminated with an optimized target marking and slight modifications in the total station's hardware (cf. section 7).

Thinking of obstacles in the line of sight - the main reason for changing reflector pole heights, the described system does not work if the target markings at the fixed part of the reflector pole (cf. section 1.3) are covered by an object. This issue cannot be solved for the described prototype and a possible market-ready successor based on the same operating principle (cf. section 2). However, the system is not meant as a substitute for manually reading the heights at the pole but as an augmentation system. In cases of obstructed target markings, the system can still inform the observer to draw special attention to the set reflector pole height.

The basic idea of the proposed system, i.e. using the ATR module and the wide-angle camera for verifying reflector pole heights, may be implemented in any robotic total station equipped with an automated fine aiming module like the ATR and a built-in wide-angle camera. Examples are the *Topcon IS-3 Imagine Station* (Topcon, 2012) or the *Trimble S8 Total Station* (Trimble, 2011).

7 Suggestions for product design

The development of a market-ready system is only possible in cooperation with the manufacturer. The assembling of a modified reflector pole is rather simple. Using a Leica GRZ122 360° prism as the main prism and a modified Leica GRZ101 360° mini reflector (Leica, 2012, pp. 23-24) as the auxiliary prism results in the example depicted in figure 7-1.

Since the auxiliary prism and the target marking for the WAC-based height verification are mounted on the fixed part of the pole, they need an aperture to allow a moving of the flexible part of the pole. Thus, the 360° mini reflector needs to be modified where a concept of a 360° prism with such an aperture already exists (Leica GRZ122 360° prism). An alternative would be to attach a prism ring as used by the Trimble I.S. Rover (Trimble, 2006).

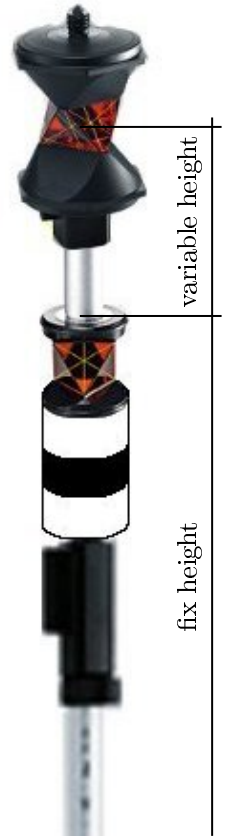

Figure 7-1: Design study of a modified reflector pole

The processing of the data (or even the measurement itself, e.g. reading the ATR values) requires access to restricted components of the total station. A short example: the measurement of the reflector pole height using the WAC-based method is possible from GeoCOM commands published in Leica (2010b) and knowledge in marker detection algorithms. However, to actually detect the marker in the image, the image needs to be transferred from the total station to a PC first. Using a serial port connection, this takes over 2 minutes for the maximum resolution of 2560 × 1920 pixel which is unacceptable for practical purposes. Processing the image inside the total station easily solves this problem. The marker detection routine described in section 4.3 also works for videos or live streams where a fast processing of the single frames is absolutely inevitable. The processing of a live stream rather than a single image is necessary for verifying the reflector pole height on the fly while being in tracking mode.

For a market-ready system, the gap in the operating range for a maximum reflector pole height of 2.15 m needs to be eliminated (no height measurements possible from 25 to 100 m, cf. section 5.3). The problem results from the small usable field of view of the ATR module (max. 0.7 gon separation between the centres of two prisms, cf. section 3.11) and the short operating range of the WAC-based height verification (25 m, cf. section 5.2).

The minimum distance for the ATR-based height verification could be improved by increasing the ATR module's field of view. In generic polar measurements, the ATR module reports an error if more than one prism is found within the field of view. Thus, increasing the field of view does not seem reasonable since the probability of spotting more prisms is also increased. Without changing the ATR module's hardware, the minimum

distance can be improved by minimizing the separation of the auxiliary prism (mounted on the fixed part of the pole) to the flexible part. However, this can lead to problems at long distances due to an overlapping of the prism spots on the CMOS array (cf. section 3.10). Changes in the ATR module's software could reduce this problem.

It is believed, that the major contribution for closing the gap in the operating range is achieved by increasing the maximum distance of the WAC-based height verification. In section 5.2, the factor limiting the maximum distance was found to be a disturbance of the marker's border by surrounding pixel. Increasing the border width from 1 cm to 2 cm increased the maximum distance from 25 m to 40 m. Since the horizontal pixel coordinates of the fiducial marker are unused in the computation of the height, it may be replaced by the target marking depicted in figure 7-1. In combination with 360° prisms, this allows a verification of the reflector pole height from any direction. Of course, the marker detection routine needs to be modified so that it searches for horizontal edges. To speed up this process and to reduce the probability of detecting false markers (cf. section 5.2), it is recommended to use only parts of the image where the known pixel coordinates of the main prism can be used for extracting them. The black and the white cylinders of the target marking depicted in figure 7-1 need a sufficient height to avoid a disturbance by surrounding pixel. Using the built-in camera at the highest resolution (2560×1920 pixel), one pixel corresponds to roughly 1 cm at a distance of 100 m (field of view of a single pixel: 6.8 mgon). Thus, it is presumably necessary to increase the camera's resolution to detect markers at long distances.

Apart from estimating the error in the angle between the optical axes of the telescope and the camera (cf. section 5.2), no additional correction of the used sensors was needed. On the part of the manufacturer, this angle needs to be calibrated once. If it is found to change with time, a simple check routine may be added to the existing ones (e.g. check routines for the collimation error or vertical index error).

A final improvement may be the replacement of the white cylinders of the target marking (figure 7-1) by an electroluminescent tape to offer WAC-based measurements in the dark. Such a tape is used by Brunner and Woschitz (2004) for the development of a "self-illuminated levelling staff". The necessary power supply could be hidden inside the pole.

Summarizing, the development of a system for the *automated, total station-based verification of reflector pole heights* is believed to be cost-efficient since, except for an improved wide-angle camera, no modifications in the hardware of an existing total station have to be made. Furthermore, the changes in the current software are manageable and therefore the proposed method may become standard in the future.

A Changes in ARToolKitPlus source code

Use double precision By default, ARToolKitPlus performs its computations using singe precision (`float`) which is especially useful for portable devices with low processing power. To use double precision (`double`), the following change has to be made.

/include/ARToolKitPlus/config.h

```
#define _USE_DOUBLE_ //add this line
#ifdef _USE_DOUBLE_
 typedef double ARFloat;
#else
 typedef float ARFloat;
#endif
```

Don't create a lookup table By default, ARToolKitPlus computes a lookup table for the distortion values during the initialization phase. This is especially useful when tracking a marker, i.e. when processing a large number of images since the distortion values for the marker's image coordinates don't have to be computed each time but are read from the lookup table. When corrections for distortions are not needed or when processing only one image, it is much faster to compute the distortion values for selected points than creating a lookup table for the whole image. The creation of a lookup table and the automatic output of the read camera parameters may be disabled by the following modifications.

src/TrackerImpl.cpp

```
AR_TEMPL_FUNC void
AR_TEMPL_TRACKER::setCamera(Camera* nCamera)
{
 arCamera = nCamera;
 if(arCamera)
 {
  arCamera->changeFrameSize(screenWidth,screenHeight);
  arInitCparam(arCamera);
  //arCamera->logSettings(logger); // comment this line
  //buildUndist02ITable(arCamera); // comment this line
 }
}
```

Sharper check on the marker's squareness Especially windows of buildings are very likely to be detected as false markers. The below modification causes a sharper check on the squareness of possible markers which reduces the probability of passing

wrong markers to the program calling the function. For the marker detection, the function `arDetectMarkerLite` was used. When using `arDetectMarker` instead (uses tracking history, only useful for detecting markers in videos), the below changes have to be made in the corresponding function.

src/core/arDetectMarker.cpp

```
AR_TEMPL_FUNC int
AR_TEMPL_TRACKER::arDetectMarkerLite(uint8_t *dataPtr, int _thresh,
   ARMarkerInfo **marker_info, int *marker_num)
{
 int16_t *limage = NULL;
 int     label_num;
 int     *area, *clip, *label_ref;
 .
 .
 .
 marker_info2 = arDetectMarker2(limage, label_num, label_ref, area,
   pos, clip, AR_AREA_MAX, AR_AREA_MIN,
   0.3, &wmarker_num); // change the former value 1.0 to 0.3
 .
 .
 .
}
```

References

Bayer G, Hinderling J, Ghesla H (2000): Process and device for rapid detection of the position of a target marking. U.S. Patent No. 6,031,606. 9p.

Bayoud FA (2006): Leica Geosystems Total Station Series TPS1200, White Paper. Leica Geosystems AG, Heerbrugg, Switzerland. 12p.

Bayoud FA (2007): Leica TPS1200+ A Telescope with Opto-Meachnical Design, White Paper. Leica Geosystems AG, Heerbrugg, Switzerland. 8p.

Bradski G, Kaehler A (2008): Learning OpenCV, 1st Edition. O'Reilly. 555p.

Brunner FK, Woschitz H (2004): Die selbstleuchtende Nivellierlatte. Allgemeine Vermessungsnachrichten 111: 104-109.

Ellison SLR, Barwick V, Farrant TJ (2009): Practical Statistics for the Analytical Scientist: A Bench Guide, 2nd Edition. RSC Publishing. 268p.

Favre C, Hennes M (2000): Zum Einfluss der geometrischen Ausrichtung von 360°-Reflektoren bei Messungen mit automatischer Zielerfassung. VPK 2/2000: 72-78.

HandheldAR (2012): Website of the Christian Doppler Laboratory for Handheld Augmented Reality at TU Graz. *http://handheldar.icg.tugraz.at* (visited in September 2012).

HITLab (2012): Website of the ARToolKit project maintained by the Human Interface Technology Laboratory (HITLab) at University of Washington. *www.hitl.washington.edu/artoolkit/* (visited in September 2012).

Joeckel R, Stober M, Huep W (2008): Elektronische Entfernungs- und Richtungsmessung und ihre Integration in aktuelle Positionierungsverfahren, 5. Auflage. Wichmann. 526p.

Kato H, Billinghurst M (1999): Marker Tracking and HMD Calibration for a video-based Augmented Reality Conferencing System. In: Proceedings of the 2nd International Workshop on Augmented Reality (IWAR 99), San Francisco, USA, October. 10p.

Kraus K (2004): Photogrammetrie: Geometrische Informationen aus Photographien und Laserscanneraufnahmen, Band 1, 7. Auflage. deGruyter. 516p.

Leica (2006): Advanced TPS Robotics, System 1200 Newsletter - No. 44. Leica Geosystems AG, Heerbrugg, Switzerland. 4p.

Leica (2010a): Leica Viva Controller CS10 & CS15 Datasheet. Leica Geosystems AG, Heerbrugg, Switzerland. 2p.

Leica (2010b): Leica TS11/TS15 GeoCOM Reference Manual, Version 2.00. Leica Geosystems AG, Heerbrugg, Switzerland. 223p.

Leica (2010c): Leica Viva TS15 Datasheet. Leica Geosystems AG, Heerbrugg, Switzerland. 4p.

Leica (2010d): Leica TS11/TS15 User Manual, Version 1.0. Leica Geosystems AG, Heerbrugg, Switzerland. 216p.

Leica (2012): Leica Geosystems Original Accessories - Material matters. Leica Geosystems AG, Heerbrugg, Switzerland. 38p.

Lienhart W, Zogg HM, Nindl D (2009): Innovative Lösungen zur Erreichung höchster Genauigkeit und Geschwindigkeit am Beispiel der TS30 Totalstation von Leica Geosystems. AVN 11-12/2009: 374-381.

Litwiller D (2001): CCD vs. CMOS: Facts and Fiction. Photonics Spectra 1/2001. 4p.

Mao J, Nindl D (2009): Surveying Reflectors - White Paper, Characteristics and Influences. Leica Geosystems AG, Heerbrugg, Switzerland. 13p.

Niemeier W (2008): Ausgleichungsrechnung: Statistische Auswertemethoden, 2. Auflage. De Gruyter. 493p.

Nindl D (2010): Surveying Tribrachs - White Paper, Characteristics and Influences. Leica Geosystems AG, Heerbrugg, Switzerland. 10p.

OpenCV (2012a): Documentation of the OpenCV project. *http://docs.opencv.org/* (visited in September 2012).

OpenCV (2012b): The OpenCV Reference Manual, Release 2.4.1. 639p.

Schweighofer G, Pinz A (2005): Robust Pose Estimation from a Planar Target. In: Proceedings of the 1st Austrian Cognitive Vision Workshop, vol. 186 of OCG Schriftenreihe: 51-58.

Stempfhuber W, Kirschner H (2008): Kinematische Leistungsfähigkeit von zielverfolgenden Tachymetern - Ein Beitrag zum Stand der Technik am Beispiel des Leica TPS1200+. AVN 6/2008: 216-223.

Topcon (2012): Topcon IS-3 Imaging Station Datasheet. Topcon Corporation, Livermore, California. 4p.

Trimble (2006): The Trimble I.S. Rover: Trimble's Integrated Surveying system. Trimble Navigation Limited, Sunnyvale, California. 4p.

Trimble (2011): Trimble S8 Total Station Datasheet. Trimble Navigation Limited, Sunnyvale, California. 4p.

Wagner D, Schmalstieg D (2007): ARToolKitPlus for Pose Tracking on Mobile Devices. Computer Vision Winter Workshop 2007, St. Lambrecht, Austria, February 6-8. 8p.

Woschitz H (2003): System Calibration of Digital Levels: Calibration Facility, Procedures and Results. PhD thesis, Institute of Engineering Geodesy and Measurement Systems, TU Graz. 222p.

Zogg HM, Lienhart W, Nindl D (2009): Leica TS30, White Paper. Leica Geosystems AG, Heerbrugg, Switzerland. 12p.